The relative importance of wind and hydroclimate drivers in modulating ~~windblown~~ the interannual variability of dust emissions in Earth system models

Xinzhu Li[1], Longlei Li[2], Yan Feng[3], and Xin Xi[1]

[1]Department of Geological and Mining Engineering and Sciences, Michigan Technological University, Houghton, MI, USA
[2]Department of Earth and Atmospheric Sciences, Cornell University, Ithaca, NY, USA
[3]Environmental Science Division, Argonne National Laboratory, Lemont, IL, USA

Correspondence: Longlei Li (ll859@cornell.edu) and Xin Xi (xinxi@mtu.edu)

Abstract. Windblown dust emissions are governed by near-surface wind speed and soil erodibility, the latter ~~influenced by hydroclimate conditions~~ modulated by hydroclimate and land use ~~. Accurate representations of the influence of these drivers in Earth system models is critical~~ conditions. Accurate model representations of these drivers are essential for reproducing historical dust variability and projecting ~~dust responses to future climate and land-use changes. Here we evaluate the model consistency in simulating the interannual variability of dust emissions and quantify the variance explained by wind speed and hydroclimate drivers within~~ future dust changes. Recognizing the unobservable, model-specific nature of dust emission fluxes, this study evaluates the discrepancies among 21 Earth system models ~~and three climate zones (hyperarid, arid and semiarid)~~in representing the relative influences of wind speed versus hydroclimate drivers on the interannual variability of dust emissions. In the hyperarid climate zone, the models ~~exhibit~~ show poor agreement in simulated dust variability, with only 10% out of 210 pairwise comparisons showing significant positive correlations. In arid and semiarid zones, the models display a ~~dipole~~ dual pattern driven by a "double-edged sword" effect of land surface memory: models with coherent hydroclimate variability show improved agreement, whereas those with divergent hydroclimate representations show ~~increased disagreement. Most models~~ larger disagreement. The models mostly capture the dominant ~~influence of wind speed on dust emissions in hyperarid areas except GFDL-ESM4 and CESM2-CAM-Kok, which display large spatial variability and anomalously high sensitivity to soil moisture and precipitation, respectively. Incorporating~~ wind control over the hyperarid zone, but show great discrepancies in the relative importance of wind versus hydroclimate drivers over arid and semiarid zones. GFDL-ESM4 and CESM2-CAM-Kok overestimate the hydroclimate influence in the hyperarid zone. Implementing the Kok et al. (2014) dust scheme in CESM and E3SM generally ~~amplifies the dust sensitivity to hydroclimate drivers and reduces the wind contribution to explained variance~~reduces wind contributions to dust variability, e.g., from 56% to ~~46% for~~ 44% in CESM and from 86% to ~~75% for E3SM in~~ 74% in E3SM within the arid zone. These findings underscore the need to improve ~~the representations of~~ near-surface ~~winds~~ wind simulations in hyperarid areas and ~~hydroclimate and land surface processes~~ land surface process representations in arid and semiarid areas to reduce ~~model~~ uncertainties in dust emission ~~estimates~~simulations.

1 Introduction

Windblown dust aerosol is an essential element of the Earth's biogeochemical cycle ~~, but~~ and has become a global concern due to its wide-ranging impacts on the climate, ecosystems, agriculture, and society. Dust emission is modulated by ~~a number of atmospheric and land surface variables which can be grouped into three broad drivers: sediment supply, sediment availability , and wind erosivity,~~ near-surface wind speed and the abundance and availability of fine soils, which collectively determine the timing, location, duration, ~~intensity, and impacts~~ and intensity of dust events (Xi, 2023). The most abundant ~~*sediment supply* is~~ fine sediments are typically found in ~~low relief~~ low-relief areas with thick ~~layers of fine, unconsolidated materials generated via~~ accumulations of unconsolidated materials produced by weathering, fluvial, and/or aeolian processes (Bryant, 2013). The ~~*sediment availability* for airborne~~ sediment availability for dust production is ~~strongly affected by~~ influenced by environmental conditions such as surface soil moisture and ~~surface~~ armoring (e.g., vegetation, soil crust~~, non-erodible coarse particles~~) which determine the minimum or ~~*threshold wind velocity* required to initiate dust mobilization (Bullard et al., 2011) . To initiate dust emission, near-surface winds must be strong enough to exceed the~~ threshold wind velocity ~~. As a result, the *wind erosivity* is dominated by infrequent, high wind events which generate sufficient drag~~ that must be reached to mobilize soil particles ~~via saltation and sandblasting mechanisms. Depending on the relative importance of the three drivers, dust emission may fall into one of three distinct regimes: *supply-limited*, where a lack of suitable-sized sediments restricts dust emission; *availability-limited*, where fine sediments are present but protected against erosion; and *transport capacity-limited*, where sediments are dry and exposed but near-surface winds are too weak to mobilize the particles.~~

~~The three dust emission drivers~~ (Bullard et al., 2011). The environmental controls of dust emissions have been incorporated in ~~global aerosol-climate models and~~ Earth system models (ESMs) to ~~capture the environmental controls on the dust cycle. Dust emission schemes in many ESMs use a~~ project dust aerosol responses to climate variability and change. Specifically, the horizontal saltation flux is parameterized as the third or fourth power of wind speed, reflecting the dominant role of infrequent, high-wind events. Many ESMs use prescribed, time-invariant dust source ~~function to represent the~~ functions to represent spatially varying sediment ~~supply~~abundance, with high values ~~generally associated with topographic depressions containing abundant alluvial or lacustrine deposits (Ginoux et al., 2001; Prospero et al., 2002; Zender et al., 2003). These areas are generally assumed to have an unlimited sediment supply,~~ assigned to low-relief areas which experience frequent dust activity as observed by satellites (Ginoux et al., 2001; Prospero et al., 2002; Zender et al., 2003). The sediment abundance is typically assumed to be unlimited without accounting for depletion or replenishment over time (Zhang et al., 2016a). ~~The~~ In ESMs, sediment availability is ~~strongly coupled with the hydroclimate variability in ESMs. Specifically, a~~ closely coupled with hydroclimate and land surface processes. Surface soil moisture, as simulated by land surface schemes, is directly used to determine the threshold wind velocity for saltation (e.g., Fécan et al., 1999). The bare soil fraction ~~scaling factor is often~~ is used to exclude non-erodible surfaces covered by snow, ice, water bodies, or vegetation. Vegetation also increases the surface roughness and reduces the wind ~~stress acting on erodible surfaces, which~~ shear stress exerted on exposed soils (Marticorena and Bergametti, 1995; Shao et al., 2011). This effect can be represented ~~by a drag partitioning scheme (Marticorena and Berga . In addition, ESMs incorporate the role of soil moisture in enhancing the threshold wind velocity or suppressing dust emissions~~

if the soil water content exceeds a given threshold (e.g., Fécan et al., 1999). Finally, ESMsparameterize the horizontal dust flux as the third or fourth power of wind speed once the threshold wind velocity is reached. This nonlinear relationship, combined with the skewed distribution of wind speeds, reflect the dominant contributions of rare, high-wind events to global dust emissions (Cowie et al., 2015; Bergametti et al., 2017). Representing dust-producing wind events in ESMs remains a major challenge, since peak-wind generation mechanisms (such as convective downdrafts) often occur at spatial scales smaller than the typical grid spacing of ESMs (Cakmur et al., 2004; Grini et al., 2005; Ridley et al., 2013; Zhang et al., 2016b). using drag partitioning schemes but is currently not considered in most ESMs.

The Numerous studies have evaluated the consistency and performance of current ESMs in simulating the global dust cycle under the Aerosol Comparisons between Observations and Models (AeroCom) initiative and Coupled Model Intercomparison Project (CMIP) have facilitated the intercomparison of ESMs in simulating the global dust cycle (Textor et al., 2006; Huneeus et al., 2011; . Generally, the (Textor et al., 2006; Huneeus et al., 2011; Kim et al., 2014; Wu et al., 2020; Gliß et al., 2021; Zhao et al., 2022; Kim et al., . Overall, modern-day dust aerosol column burden is reasonably constrained by ground- and satellite-based aerosol optical depth (AOD) observationsover continental outflow areas, resulting in , leading to better model agreement compared to than that in dust emission and deposition estimates. Knippertz and Todd (2012) suggested that model tunings tuning to match satellite observations, e.g., via the use of prescribed dust source functions, induce induces a compensational effect between dust emission and deposition, both of which lack robust observational constraints at global scalesthe global scale. Indeed, previous AeroCom and CMIP model intercomparisons consistently show large discrepancies in the global total and regional distribution of dust emissions (Huneeus et al., 2011; Wu et al., 2020; Gliß et al., 2021; Zhao et al., 2022). While most ESMs roughly capture the annual cycle of dust over major source regions, they struggle past studies have reported persistent, substantial model discrepancies in global dust emission estimates and difficulties in reproducing the dust interannual variability and relationships with historical dust variability and its dependence on wind speed and soil bareness (Pu and Ginoux, 2018; Evan et al., 2014; Evan, 2018; W . Recent studies suggested that all CMIP models bare soil fraction (Huneeus et al., 2011; Evan et al., 2014; Evan, 2018; Pu and Ginoux, 201 . More recently, Kok et al. (2023) suggested that current ESMs failed to capture the large increase of global dust burden since preindustrial times, likely due to inaccurate model representations of historical representations of the climate and land-use changes drivers of dust emissions, and/or the dust sensitivity to these changes Kok et al. (2023); Leung et al. (2025). Together, these studies underscore the persistent uncertainties and limited predictive capability of ESMs in simulating the response of windblown dust emissions to hydroclimate variability and land surface changesdrivers in these models.

The model discrepancies can be explained, at least in part, by the choice of dust emission schemes. Earlier-generation schemes relied on empirical, temporally-invariant Earlier schemes rely on prescribed, time-invariant dust source functions to shift emissions towards satellite-observed hotspot regions (Ginoux et al., 2001; Zender et al., 2003), whereas newer schemes adopt more mechanistic approaches that account for represent sediment availability as a function of land surface conditions, thereby eliminating the need for dust prescribed source functions (Kok et al., 2014b). These process-based schemes also introduce more realistic parameterizations of With improved model physics, however, newer schemes require a larger set of input parameters that may introduce additional uncertainties. In addition, some schemes explicitly represent sandblasting efficiency to represent describe the momentum transfer from saltating soil grains to the entrainment of fine particles

dust entrainment into the atmosphere ~~(Zender et al., 2003; Kok et al., 2014b). With improved model physics, process-based schemes usually involve more extensive input parameters with greater uncertainties~~(e.g., Zender et al., 2003; Kok et al., 2014b) , while simplified approaches assume a linear scaling between the vertical and saltation dust fluxes (e.g., Ginoux et al., 2001; Volodin and K
. The choice of wind speed also varies: some schemes use 10-m ~~wind speeds~~ winds for simplicity, while others use friction velocity, which ~~better~~ more accurately captures the wind stress acting on soil surfaces but requires information on surface roughness. Because surface roughness length is poorly constrained by observations, models ~~employ~~ rely on varying assumptions and tunings to account for its effects on dust ~~emission~~ emissions (e.g., Peng et al., 2012; Albani et al., 2015; Tegen et al., 2019).

Even ~~with~~ when using the same dust scheme, ESMs can diverge substantially ~~due to~~ in dust emission simulations because of differences in model configurations (e.g., horizontal resolution, vertical levels), parameter tunings, and coupled physical parameterizations. For instance, the bare soil fraction is determined from land type, vegetation fraction, and snow ~~areal~~ area extent, all of which may differ ~~between~~ across ESMs. In particular, vegetation cover may be prescribed from ~~a fixed~~ satellite climatology or simulated interactively ~~. Further discrepancies may~~ within the model. Dust emission discrepancies may also result from differences in soil properties (e.g., hydraulic conductivity), soil column structure (e.g., number and thickness of layers), and hydrologic processes (e.g., precipitation, runoff, evaporation), which ultimately determine the ~~water content of top soil layers and consequently the threshold wind velocity~~surface soil moisture and erodibility. The soil moisture effect on threshold wind velocity is also treated ~~inconsistently, e.g., in calculating the residue~~ in different ways, for example, in how models define the residue moisture level below which soil ~~moisture~~ wetness is assumed to have no ~~effects on dust emission (e.g., Fécan et al., 1999; Evans et al., 2016; Volodin and Kostrykin, 2016)~~effect (e.g., Fécan et al., 1999; Ginoux et al., 2001; Evans et al., . Moreover, ESMs ~~employ different parameterizations for planetary boundary layer and subgrid processes, which affect the momentum transfer from the atmosphere to the surface. Because of the strong coupling between dust emission and boundary layer and land surface processes~~differ in the parameterizations for convection and atmospheric boundary layer processes, both of which strongly influence the generation of peak low-level winds. Therefore, it is not surprising that dust emission estimates are strongly model-dependent, considering the tight coupling between dust emission and the broader model physics and configurations.

While ~~past studies have documented the large model diversity in the climatological dust cycle (e.g., Pu and Ginoux, 2018; Wu et al., 2020 , key questions remain as to whether current ESMs consistently capture the temporal variability of historical~~ model discrepancies in global dust emission estimates are well documented in past studies, a key question remains as to how consistently and accurately current ESMs capture the interannual variability of dust emissions and their ~~sensitivities to wind and hydroclimate~~ sensitivity to physical drivers. Addressing ~~these questions~~ this question is essential for understanding and reducing model uncertainties in projecting dust ~~emission~~ responses to future ~~changes in climate and land use~~climate and land-use changes. In this study, we ~~provide a detailed assessment of~~ evaluate the interannual variability ~~and physical drivers of dust emissions, by quantifying the inherent~~ of dust emission fluxes and quantify the relative influence of near-surface wind ~~speed and hydroclimate conditions in modulating the dust variability within~~ and hydroclimate drivers simulated by a suite of state-of-the-art ESMs. Compared ~~to previous studies, we shift~~ with previous work, our analysis shifts the focus from climatological means to temporal

variability and ~~move~~ moves beyond documenting uncertainties to diagnosing their physical origins, thereby ~~offering critical~~ providing new insights for improving ~~the dust representation~~ dust emission representations in ESMs.

A major challenge in evaluating dust models is the lack of direct ~~, global~~ observational constraints on dust emission fluxes. While ~~satellite-derived dust optical depth and long-term surface concentration records~~ satellite-based dust AOD and in-situ dust concentration measurements provide valuable insights into dust variability (e.g., Prospero and Lamb, 2003; Zender and Kwon, 2005; Ginoux et al., 2012), they integrate ~~information from~~ the effects of emission, transport, and deposition, making it difficult to isolate the emission process (the focus of this ~~work). Therefore~~study). Thus, rather than validating ~~absolute~~ model performance against observations, we focus on diagnosing the inter-model consistency ~~of simulated~~ in dust emission variability ~~. Here we treat model-simulated~~ across different climate zones (i.e., hyperarid, arid and semiarid). In contrast to previous studies, we treat dust emission flux as an unobservable, model-specific quantity ~~, which is characterized by a dynamic range defined by the internal model variability, parameterizations, parameter uncertainties, and model configurations. This approach is analogous~~ in our study, similar to Koster et al. (2009)'s view of root-zone soil moisture~~and reflects~~ . This perspective recognizes the fact that ~~model-simulated~~ simulated dust emission fluxes cannot be directly validated with field observations~~.~~ ~~While model-simulated dust emissions are essentially approximations of the true state they aim to reproduce, their~~ , and are characterized by a dynamic range defined by each model's physical parameterizations, parameter uncertainties, and structural configurations. The true information content ~~lie~~ of model-simulated dust emission fluxes therefore lies not necessarily in ~~the absolute magnitudes~~their absolute magnitudes, but in their spatiotemporal variability and sensitivities to physical drivers. ~~By quantifying the relative influence of wind speed and hydroclimate conditions over different climate regimes (i.e., hyperarid, arid and semiarid), this study provides new insights into model discrepancies and biases in dust emission representations.~~

The remainder of this paper is organized as follows. Section 2 describes the ESMs and reanalysis datasets considered in this study, and the dominance analysis technique used to quantify the joint and relative ~~influence~~ influences of dust emission drivers. Section 3 presents the ~~intercomparison~~ model comparison of dust interannual variability and ~~the~~ relative influence of wind ~~speed and hydroclimate conditions. The conclusions are summarized in Section 4.~~ and hydroclimate drivers. Section 4 summarizes the main conclusions.

2 Data and Approach

2.1 ESMs and aerosol reanalysis ~~products~~

~~Table 1 summarizes the ESMsand reanalysis products analyzed in this study, which differ in model resolution, vegetation process, and dust emission parameterizations, among other aspects. Among the 21 ESMs,~~ We consider a total of 21 ESMs, summarized in Table 1. These include 18 ~~are~~ models from the CMIP6 ~~historical, fully-coupled experiments~~ fully coupled historical experiment (1980–2014). ~~We~~ For each model, we use the first ensemble member (r1i1p1f1) ~~from each model,~~ unless otherwise stated. ~~CMIP6 consists of several model families that share common heritage but differ in physics options and configurations. For instance, two Community Earth System Model (CESM) configurations~~ Two CESM variants employ the dust ~~scheme~~ emission parameterization of Zender et al. (2003) (hereafter the Zender scheme) but use different atmo-

Table 1. Summary of the Earth system models and aerosol reanalysis datasets considered in this study. Dust source function (DSF) column indicates whether ~~an empirical~~ a prescribed dust source function is used. Leaf area index (LAI) column indicates whether LAI is treated as a prognostic variable. D_m, dust particle diameter upper limit.

Model	Resolution	D_m	Wind	DSF	LAI	Dust Scheme	Referenc
~~CESM2-CAM-Zender~~ CESM2-WACCM-Zender	0.9°×1.25°	10	u_*^3	Y	Y	Zender et al. (2003)	~~Albani e~~
~~CESM2-WACCM-Zender~~CESM2-CAM-Zender	0.9°×1.25°	10	u_*^3	Y	Y	Zender et al. (2003)	~~Gettelm~~
CESM2-CAM-Kok	0.9°×1.25°	10	u_*^3	N	Y	Kok et al. (2014b)	Li et al.
E3SM2-Zender	1°×1°	10	u_*^3	Y	~~Y~~ N	Zender et al. (2003)	Feng et
E3SM3-Kok	1°×1°	10	u_*^3	Y	Y	~~Zender et al. (2003)~~ Kok et al. (2014b)	Xie et al
CanESM5-1	2.8°×2.8°	Bulk	u_*^3	Y	Y	Peng et al. (2012)	Sigmond
CNRM-ESM2.1	1.4°×1.4°	20	u_*^3	N	Y	Tegen et al. (2002)	Séférian
EC-Earth3-AerChem	2°×3°	20	u_*^3	Y	N	Tegen et al. (2002)	Van Noij
GISS-E2.1-OMA	2°×2.5°	32	u_{10}^3	Y	N	Miller et al. (2006)	Miller et
GISS-E2.1-MATRIX	2°×2.5°	32	u_{10}^3	Y	N	Miller et al. (2006)	Miller et
GISS-E2.2-OMA	2°×2.5°	32	u_{10}^3	Y	N	Miller et al. (2006)	Rind et
GFDL-ESM4	1°×1.25°	20	u_*^3	Y	Y	Ginoux et al. (2001)	Shevliak
HadGEM3-GC31	0.6°×0.8°	63	u_*^3	Y	N	Woodward (2011)	Roberts
UKESM1.0	1.25°×1.9°	63	u_*^3	N	Y	Woodward (2001)	Woodwa
INM-CM5.0	1.5°×2°	Bulk	u_*^4	N	N	Volodin and Kostrykin (2016)	Volodin
IPSL-CM6A-LR	1.26°×2.5°	Bulk	u_{10}^3	Y	Y	Balkanski et al. (2004)	Lurton e
MRI-ESM2.0	1.9°×1.9°	20	u_*^3	N	N	Shao et al. (1996)	Yukimot
MIROC6	1.4°×1.4°	10	u_{10}^3	N	Y	Takemura et al. (2009)	Tatebe e
MIROC-ES2L	2.8°×2.8°	10	u_{10}^3	N	Y	Takemura et al. (2009)	Hajima
MPI-ESM-1.2	1.9°×1.9°	Bulk	u_*^3	Y	Y	Cheng et al. (2008)	Mauritso
NorESM2	0.9°×1.25°	10	u_*^3	Y	N	Zender et al. (2003)	Seland e
MERRA2	0.5°×0.63°	20	u_{10}^3	Y	N	Ginoux et al. (2001)	Randles
JRAero	1.1°×1.1°	20	u_*^3	N	N	Shao et al. (1996)	Yumimo

spheric schemes: the Community Atmosphere Model (CESM2-CAM-Zender) ~~vs.~~ versus the Whole Atmosphere Community Climate Model (CESM2-WACCM-Zender)~~, with major differences in the vertical extent and upper atmospheric processes. Three GISS-E2 models use the same dust scheme of Miller et al. (2006) but differ in model version (2.1 vs. 2.2) and aerosol microphysics schemes: One-Moment Aerosol (OMA; ensemble member r1i1p3f1) vs. Multiconfiguration Aerosol TRacker of mIXing state (MATRIX; ensemble member r1i1p5f1) (Miller et al., 2021; Rind et al., 2020). UKESM1.0 is built upon the HadGEM3-GC3.1 general circulation model, which use the same dust scheme of Woodward (2001) but differ in parameter tunings and dust source representations (Woodward et al., 2022). Similarly, MIROC-ES2L is based on the MIROC general circulation model version 5.2~~ . We also performed a separate CESM simulation (~~MIROC5) (Hajima et al., 2020), while MIROC6 incorporates updated physics which improved the mean climate state and internal variability relative to MIROC5 (Tatebe et al., 2019) . Both MIROC-ES2L and MIROC6 adopt the dust scheme from the SPRINTARS aerosol module (Takemura et al., 2009).~~

~~In addition to the CMIP6 archive, we consider an updated CESM (~~2004–2013) coupled with the dust scheme of Kok et al. (2014b) (hereafter the Kok scheme; CESM2-CAM-Kok) (Li et al., 2022)~~, and the Energy Exascale Earth System Model (~~. In addition, we conducted two experiments using the DOE E3SM ~~, model~~ (1980–2014)~~using ~~, which are coupled with the Zender (E3SM2-Zender) and Kok schemes (E3SM3-Kok)~~schemes (Feng et al., 2022; Xie et al., 2025). The ~~, respectively (Feng et al., 2022; Xie et al., 2025). A key difference between the ~~two~~ Zender and Kok schemes is that~~the Kok scheme adopts physically based soil erodibility parameterizations and eliminates the use of empirical dust source functions unlike the Zender scheme~~, the Zender scheme relies on a prescribed, time-invariant dust source function to shift emissions towards contemporary dust source areas, whereas the Kok scheme applies more physically based parameterizations of the dust sensitivity to soil erosion thresholds, thereby improving dust simulations without the use of prescribed source functions (Kok et al., 2014a). These paired CESM and E3SM experiments allow us to evaluate how the choice of dust ~~schemes (Zender vs. Kok) or models (CESM vs. E3SM) affect dust emission simulations. Nonetheless, we should point out that~~ emission schemes and host models affect the simulated dust sensitivities to physical drivers. However, it is worth noting that CESM2-CAM-Zender does not account for dust mineralogy, whereas CESM2-CAM-Kok simulates dust as mineral components with observationally constrained mineral optical properties (Li et al., 2024)~~, whereas CESM2-CAM-Zender does not account for particle mineralogy and simulates different dust optical properties that may affect dust~~ . This may lead to different radiative feedback on meteorology ~~. Also~~and contribute to model disparity in dust emissions. Similarly, E3SM3 ~~includes extensive updates over~~ incorporates extensive model updates relative to E3SM2~~that may affect the~~ , which may affect simulations of near-surface meteorological and land surface conditions relevant to dust emissions (Xie et al., 2025).

Several other model families share common heritage but differ in physics options and configurations. For example, three GISS-E2 models use the same dust scheme of Miller et al. (2006) but differ in model version (2.1 vs. 2.2) and aerosol microphysics scheme: One-Moment Aerosol (OMA; ensemble member r1i1p3f1) versus Multiconfiguration Aerosol TRacker of mIXing state (MATRIX; ensemble member r1i1p5f1) (Miller et al., 2021; Rind et al., 2020). UKESM1.0 is developed based on the HadGEM3-GC3.1 general circulation model. They use the same dust scheme of Woodward (2001) but differ in parameter tunings and dust source representations (Woodward et al., 2022). Both MIROC-ES2L and MIROC6 use the dust scheme from the SPRINTARS aerosol module (Takemura et al., 2009). MIROC-ES2L builds upon the MIROC general circulation model

version 5.2 (MIROC5) (Hajima et al., 2020), while MIROC6 incorporates updated physics that improved the mean climate state and internal variability compared to MIROC5 (Tatebe et al., 2019).

We further compare the ~~ESMs~~ ESM simulations with two aerosol reanalysis products: Modern-Era Retrospective Analysis for Research and Applications version 2 (MERRA2, 1980–2014) (Gelaro et al., 2017), and Japanese Reanalysis for Aerosol (JRAero, 2011–2017) (Yumimoto et al., 2017). ~~MERRA2 is produced by the GEOS-5 data assimilation system with radiatively-coupled Goddard Chemistry Aerosol Radiation and Transport (GOCART) module.~~ Dust emission in ~~GOCART is represented~~ MERRA2 is simulated using the Ginoux et al. (2001) ~~scheme. JRAero is produced by the Japan Meteorological Agency MASINGAR mk-2 global aerosol transport model, which simulates dust emission~~ parameterization within the GOCART aerosol module of the GEOS-5 model. In JRAero, dust emissions are simulated using the Shao et al. (1996) energy-based scheme ~~, same as~~ (same as in MRI-ESM2.0~~(Yumimoto et al., 2017; Yukimoto et al., 2019). The meteorological and land surface conditions in~~) within the Japan Meteorological Agency MASINGAR mk-2 global aerosol transport model (Yumimoto et al., 2017; Yukimo
. In both MERRA2 and JRAero~~are constrained by observational data assimilation , and thus are expected to better capture historical climate and land cover changes than the ESMs.~~ , the meteorological inputs for dust emission calculations are generated via data assimilation of diverse in situ and remote sensing observations (including surface and upper-air wind measurements), which improves the accuracy of near-surface winds compared to free-running models (Gelaro et al., 2017; Yumimoto et al.,
. The surface soil moisture in MERRA2 ~~and JRAero also benefit from assimilation of~~ also benefits from the assimilation of observation-corrected precipitation. Although both reanalyses assimilate bias-corrected total AOD, ~~which provides some constraint on the dust column burden but does not directly constrain dust emissions~~it is expected to have limited effect on dust emission simulations.

We evaluate the consistency ~~between~~ among the ESMs and reanalysis products in ~~representing~~ simulating the interannual variability of ~~total~~ dust emission fluxes. To facilitate ~~comparison across common dust-emitting regions, we divide global dust source areas~~ regionally consistent comparisons, global dryland areas are categorized into three climate ~~zones: hyperarid~~zones—hyperarid, arid, and ~~semiarid, based on the~~ semiarid—based on aridity index (AI), defined as the ratio of ~~1970–2000~~ climatological mean precipitation to potential evapotranspiration ~~using the data from Zomer et al. (2022)~~for 1970–2000 following (Zomer et al., 2022) . The hyperarid zone is defined as AI$\leq$0.05, arid zone as 0.05<AI$\leq$0.2, and semiarid zone as 0.2<AI$\leq$0.5. ~~Using these climatologically defined zones allows us to assess model discrepancies over common dust-emitting areas. Figure 1shows that the hyperarid zone primarily covers~~ As shown in Figure 1, hyperarid areas primarily cover North Africa, Arabian Peninsula, Iranian Plateau, and Tarim Basin. Arid and semiarid ~~zones~~ areas cover other major dust sources, including the Sahel (North Africa), Turan Depression (Central Asia), Gobi Desert (East Asia), Thar Desert (South Asia), Kalahari Desert (Southern Africa), Chihuahua Desert (North America), Patagonia steppe (South America), and the Great Sandy and Simpson Deserts (Australia). The rationale ~~of this climate zone-based~~ for climate zone analysis is that the relative importance of wind ~~speed versus hydroclimate conditions~~ versus hydroclimate controls on dust emission is expected to ~~depend strongly on climate regime. Specifically, hyperarid areas are expected to be~~ vary with climate aridity. Hyperarid areas are dominated by permanently dry, barren surfaces with ~~very low~~ minimal hydroclimate variability, ~~and thus~~ so dust emission is primarily controlled by wind speed. ~~Whereas, the~~ In contrast, arid and semiarid zones ~~are expected to exhibit increased~~ experience greater precipi-

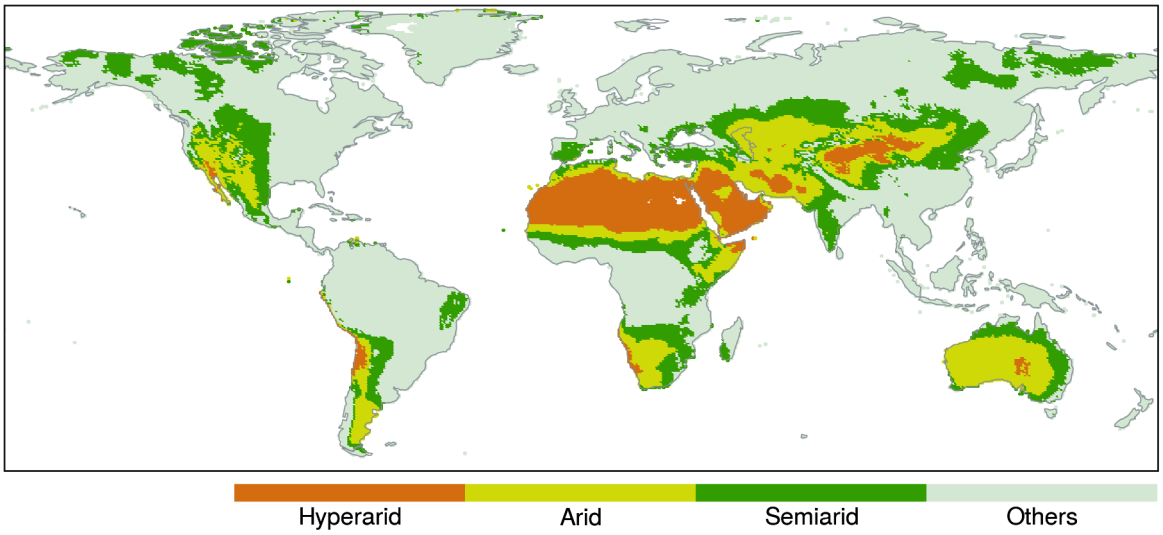

Figure 1. Definitions of hyperarid, arid, and semiarid climate zones.

tation and hydroclimate ~~variability resulting in stronger influence on the sediment availability~~fluctuations, which exert stronger influences on soil erodibility.

2.2 Dominance analysis technique

~~Past studies have~~ Previous studies have commonly used linear regression coefficients to quantify ~~dust sensitivities to its~~ the dust sensitivity to physical drivers (e.g., Pu and Ginoux, 2016; Aryal and Evans, 2021; Zhao et al., 2022). In multiple linear regression, a regression coefficient represents the mean change in the response variable ~~per~~ (e.g., dust emission flux or AOD) associated with a unit change in a given predictor, while holding all other predictors constant. This interpretation assumes mutual independence among predictors, an assumption ~~that is often~~ violated by strong correlations among hydroclimate variables. As a result, linear regression coefficients ~~may~~ can yield misleading inference ~~of predictor importance~~ regarding the relative importance of predictors. Moreover, regression coefficients, standardized or not, may not provide a ~~direct comparison of predictor influence due to the varying dynamic ranges in ESMs~~consistent basis for comparing predictor importance across the ESMs, due to inconsistent dynamic ranges of predictors among models.

In this study, we apply the dominance analysis technique to quantify the relative influence of wind and hydroclimate drivers on dust ~~variability~~emissions. Dominance analysis quantifies the marginal contribution of each predictor to the total explained variance (R^2) in the response variable by evaluating all possible subset models ($2^p - 1$ subsets for p predictors) in a multiple linear regression framework (Budescu, 1993; Azen and Budescu, 2003). For each predictor, the method calculates its average incremental contribution to the total R^2 across all subset models of the same size (i.e., models with the same number of predictors)~~, and then average these values~~. These incremental R^2 values are then averaged to obtain the predictor's ~~unique~~

overall contribution to the total R^2. A key ~~property of this method~~ feature of this approach is that the sum of individual predictor contributions equals the total R^2 of the full model (i.e., with all predictors included), thereby allowing the partitioning of explained variance among correlated predictors. The ~~predictor-specific~~ resulting predictor R^2 values ~~can thus be interpreted as the portions~~ thus represent the proportions of total variance in the response variable that ~~are uniquely and jointly~~ can be attributed to each predictor, accounting for their ~~interactions and~~ multicollinearity.

~~We use the monthly total dust emission flux~~ The monthly dust emission fluxes simulated by each ESM are used as the response variable~~and~~ . Although the models differ in how the total emission flux is partitioned into discrete size bins—a key factor influencing dust transport and atmospheric lifetime—the size partitioning has minor effects on diagnosing the emission process itself. In particular, the physical drivers considered here operate upstream of the size partitioning, and thus mainly control the initiation and magnitude of total dust emission rather than its size-resolved characteristics.

For each ESM, we consider six predictors: 10-m wind speed, total precipitation (including liquid and solid phases), water content in the uppermost soil layer (~~hereafter as~~ soil moisture), 2-m specific humidity, 2-m air temperature, and leaf area index (LAI). ~~The total dust emission flux is a bulk quantity that represents the source strength. Although ESMs differ in how they partition the total flux into discrete particle size bins—a key factor influencing dust transport and atmospheric lifetime—we expect the size partitioning to have minimal impact on diagnosing the emission process itself, particularly its sensitivity to the selected predictors . The primary drivers of emission variability operate upstream of the size partitioning of mobilized soil particles. The six predictors~~ These predictors are chosen because they are either directly used as input parameters in dust flux ~~calculations or strongly correlated with~~ parameterizations or are closely linked to dust emission intensity, as suggested in ~~numerous~~ previous studies (e.g., Engelstaedter et al., 2003; RAVI et al., 2006; Zou and Zhai, 2004; Sokolik et al., 2021; Cowie et al., 2015; Kim and Choi, 2015; Xi and Sokolik, 2015a, b; Xi, 2023). Among them, 10-m wind speed represents the wind ~~erosivity driver~~shear drag responsible for dust mobilization, while the remaining variables ~~collectively~~ represent the hydroclimate ~~effect~~ controls on sediment availability.

Dominance analysis is ~~performed for~~ applied to all ESMs and MERRA2 over grid cells with nonzero emissions~~using deseasonalized and normalized data. JRAero is excluded from the dominance analysis due to missing predictors and its short time span. We first subtract~~ . Prior to analysis, the data are first deseasonalized by subtracting month-wise climatological means from ~~the monthly dust~~ both the dust emission fluxes and predictors, and ~~then convert the deseasonalized data into~~ subsequently normalized to the 0–1 range via min-max ~~normalization. For ESMs that use bare soil fraction as a scalingfactor in dust flux calculations (e.g., CNRM-ESM2.1, INM-CM5.0, UKESM1.0), the dust flux is first normalized by the bare soil fraction in order to isolate the influence of the selected predictors. The~~ scaling. The resulting grid-level ~~total and predictor-specific~~ predictor R^2 values are then used to assess (1) the internal spatial variability ~~(i.e.,~~ of predictor importance within each climate zone and model, and (2) and inter-model consistency in ~~the total explained variance and predictor relative importance.~~ representing the predictor relative influence on the interannual dust emission variability. JRAero is excluded from this analysis due to missing predictor data.

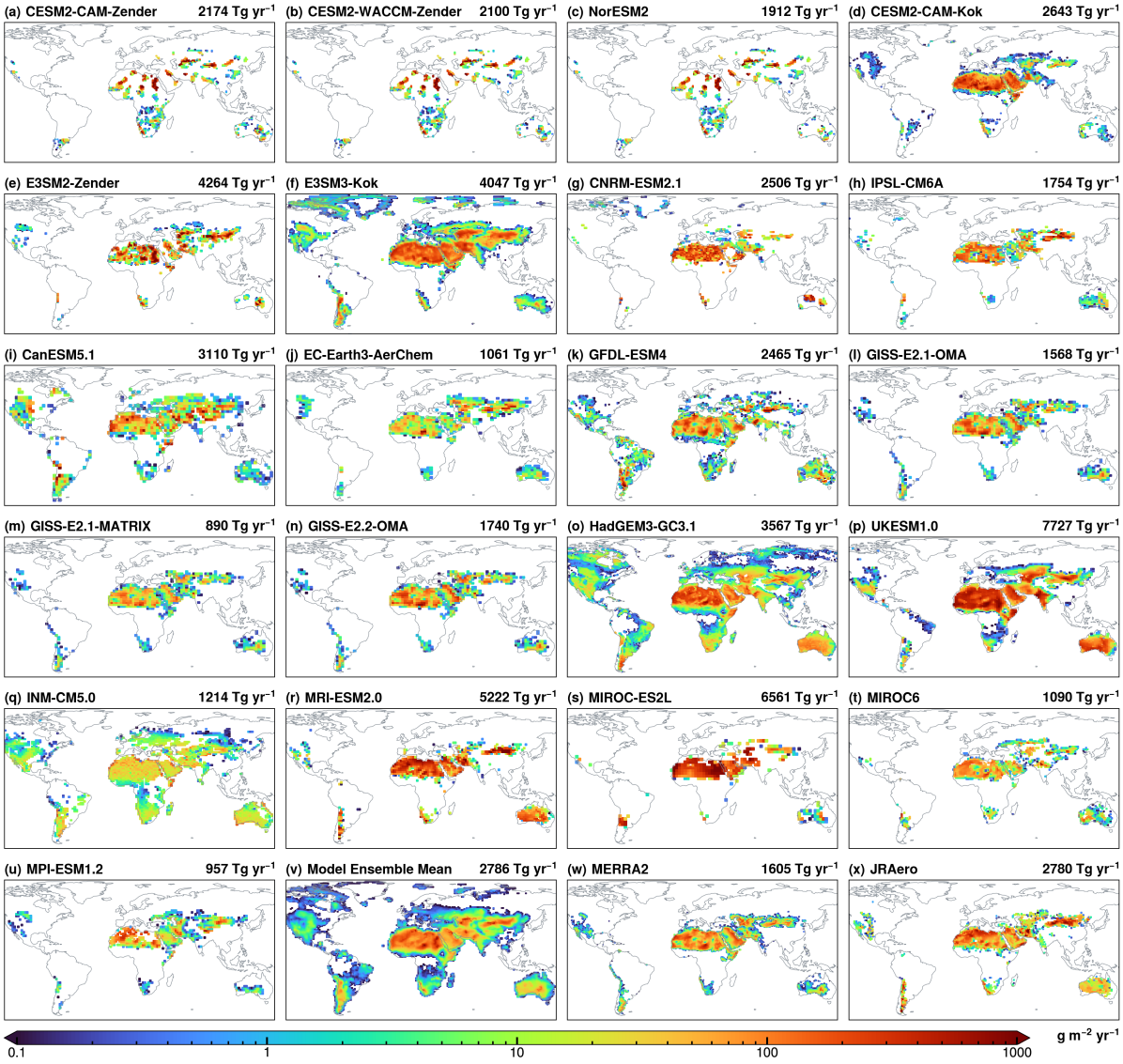

Figure 2. Climatological mean dust emission fluxes from (a–u) ~~individual~~ 21 Earth system models, (v) model ensemble mean, (w) MERRA2 reanalysis, and (x) JRAero reanalysis. Global annual total ~~dust~~ emissions are displayed on each panel.

3 Results

3.1 Climatological distribution

Figure 2 displays the climatological mean annual dust ~~fluxes from~~ emission fluxes from the 21 ESMs, ~~the model~~ their ensemble mean, and the MERRA2 and JRAero ~~datasets for the~~ reanalyses for 2005–2014 ~~period~~ (2004–2013 for CESM2-CAM-Kok and 2011–2017 for JRAero). All datasets capture the global dust belt stretching from West Africa across the Middle East to East Asia, as well as ~~the less intense~~ weaker sources in the Americas and Australia. Among the models, E3SM3-Kok and HadGEM2-GC31 simulate the most extensive dust-emitting areas~~including~~ , extending into high-latitude and subhumid areas. ~~In contrast,~~ CESM2-CAM-Zender, CESM2-WACCM-Zender ~~,~~ and NorESM2 ~~simulate discrete and limited dust-emitting areas by excluding areas with~~ restrict emissions to regions where the dust source function ~~values below~~ exceeds 0.1~~.~~, resulting in discrete and spatially limited emission areas. Conversely, E3SM2-Zender ~~uses the original , unmodified Zender et al. (2003)~~ employs the original dust source function ~~and thus produces~~ of Zender et al. (2003), producing a more spatially continuous emission pattern (Fig. 2e).

~~The global total dust flux varies greatly among the ESMs~~ Global annual dust emissions simulated by the ESMs vary greatly, ranging from 890 to 7727 Tg yr^{-1} with nearly an order of magnitude difference (Fig. 2a–2u). The ~~model~~ ensemble mean estimate ~~is 2786 Tg yr^{-1}~~ (Fig. 2v) is 2786 Tg yr^{-1} with a standard deviation of 1821 Tg yr^{-1}, corresponding to a diversity of 65% (defined as the ratio of the standard deviation to ~~model~~ the ensemble mean). Based on models with ~~a dust size upper~~ an upper particle size limit of 20 μm, global ~~dust~~ emissions vary from 1062 to 6561 Tg yr^{-1}, with a mean of 3012 Tg yr^{-1} and diversity of 51%. ~~This uncertainty range is consistent with prior~~ Compared to aerosol reanalysis data, the ensemble mean estimate is close to JRAero (2780 Tg yr^{-1}, Fig. 2x), but considerably higher than MERRA2 (1605 Tg yr^{-1}, Fig. 2w). Also, the ensemble mean exhibits a more spatially homogeneous pattern over North Africa and the Arabian Peninsula, whereas MERRA2 and JRAero display more heterogeneous and localized emission patterns.

The model discrepancies in dust emission magnitude is consistent with previous assessments. For example, Huneeus et al. (2011) compared 14 ~~models from~~ AeroCom Phase I models and reported a global dust emission range of 500–4400 Tg yr^{-1} ~~with a diversityof~~ (diversity=58%~~. Out of the 14 models, 7 models considered particle diameters up to~~), of which seven using a 20 ~~μm and reported a flux of~~ μm upper size limit yielded 980–4300 Tg yr^{-1} ~~with a diversityof~~ (diversity=46%). Similarly, Gliß et al. (2021) compared 14 AeroCom Phase III models and ~~found~~ reported a range of 850–5650 Tg yr^{-1} with a diversity of 64%. Based on 15 CMIP5 models Wu et al. (2020) reported a range of 740–8200 Tg yr^{-1} ~~with a diversityof~~ (diversity=66%~~based on 15 CMIP5 models. Out of the 15 models, 7 models considering a diameter range of 0–20 μm yielded~~), with seven models using particle diameters up to 20 μm producing 740–3600 Tg yr^{-1} ~~with a diversityof~~ (diversity=43%). More recently, Zhao et al. (2022) ~~compared~~ examined 15 ~~models from the~~ CMIP6 AMIP ~~experiment~~ models and reported a range of 1400–7600 Tg yr^{-1} ~~with a diversityof~~ (diversity=61%~~. Past studies, together~~). Collectively, these studies, along with our results, ~~indicate persistent large~~ demonstrate persistent large model uncertainties in global dust ~~emissions, despite improvements~~ emission estimates, despite advances in model resolutions ~~and physics.~~

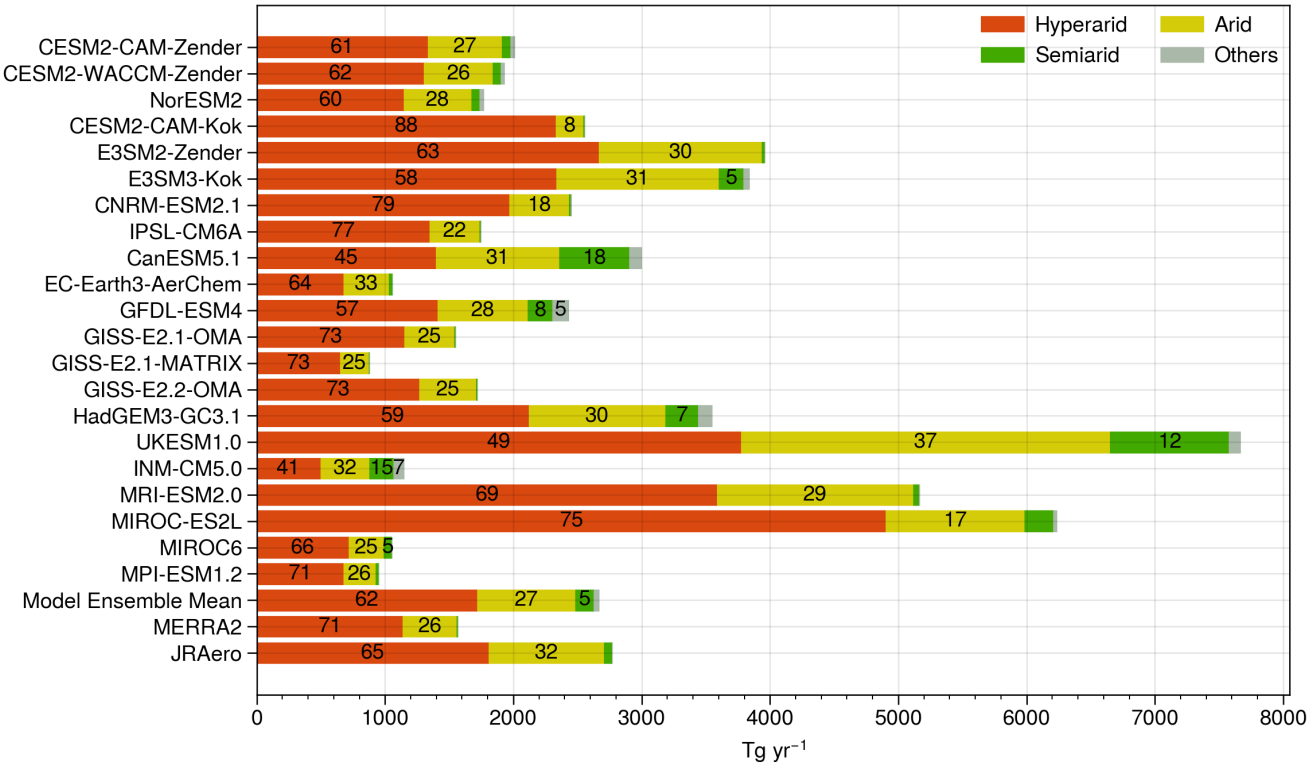

Figure 3. Contributions of different climate zones to global annual dust emissions. Numbers indicate percentages above 5%.

~~The model ensemble mean global total dust flux is significantly higher than that of MERRA2 (1605 Tg yr^{-1}, Fig. 2w), but closely aligns with JRAero (2780 Tg yr^{-1}, Fig. 2x). In general, the model ensemble mean exhibits a more spatially homogeneous pattern over North Africa and Arabian Peninsula, whereas MERRA2 and JRAero display more heterogeneous and localized patterns~~parameterizations, and process understanding.

Figure 3 displays the ~~fractional~~ contributions of different climate zones to global dust emissions. The hyperarid zone accounts for more than half of global ~~total emissions in most ESMs except two models :~~ emissions in all models except CanESM5.1 and INM-CM5.0, both of which simulate relatively uniform emission patterns with less than 50% from ~~the hyperarid zone~~ hyperarid areas (Fig. 2i, 2q). This may be ~~due to known deficiencies of these two models~~caused by known model deficiencies. As noted in Sigmond et al. (2023), improper parameter ~~tuning~~ tunings related to the hybridization of dust tracers caused spurious dust events and inaccurate dust distributions in CanESM5.1. An interpolation error in the bare soil fraction also distorted the model's dust source characterization, resulting in poor agreement with satellite observations~~(Sigmond et al., 2023)~~. In INM-CM5.0, the vertical dust flux is calculated as a function of ~~friction~~ wind velocity only, without accounting for ~~the dependence of threshold wind velocity on land surface conditions~~ land surface controls on the erosion threshold (Volodin and Kostrykin, 2016; Volodin, 2022). While this simplification may be appropriate for ~~the hyperarid~~ hyperarid climate zone, it can ~~introduce significant biases~~

overestimate dust emissions over arid and semiarid zones where ~~hydroclimate conditions play an increasingly important role in dust emissions~~increased soil wetness and armoring suppress dust mobilization.

~~Over~~ The contribution of the arid climate zone ~~, the dust emission fraction~~ ranges from 8% (CESM2-CAM-Kok) to 37% (UKESM-1.0), ~~reflecting substantial~~ indicating substantial model discrepancies compared to the hyperarid zone. The discrepancies ~~among the ESMs. These discrepancies~~ become even larger over the semiarid zone, where the ~~contribution~~ emission fraction ranges from less than 1% to 18%. ~~Three ESMs~~ Particularly, three models allocate more than 10% ~~of dust~~ to the semiarid zone: CanESM5.1 (18%), INM-CM5.0 (15%), and UKESM1.0 (12%). ~~Thus~~Overall, as the climate ~~zone shifts~~ regime transitions from hyperarid to semiarid, ~~the ESMs show larger discrepancies in their estimates of relative source strength. This climate zone-based comparison offers a first-order view of model representations of the~~ model-estimated dust source strengths become less consistent, revealing increasing uncertainty in how ESMs represent dust sensitivity to hydroclimate conditions. ~~Based on the model ensemble mean, global dust emissions are partitioned as 61% from hyperarid, 27% from arid, and 5% from semiarid zones. In contrast, MERRA2 and JRAero produce most dust from hyperarid and arid zones, with negligible contributions from the semiarid zone.~~

Among the ESMs, CESM2-CAM-Zender ~~, CESM2-WACCM-Zender and NorESM2 produce similar~~ and CESM2-WACCM-Zender produce nearly identical total emissions and ~~regional fractions~~spatial distributions, suggesting that the choice between CAM and WACCM ~~has minimal influence when the same dust scheme (Zender) is used~~atmospheric components has minimal effect. The paired CESM and E3SM experiments~~show different changes in regional fractions. For instance, the hyperarid zone fraction~~ , however, show opposite tendencies: the hyperarid-zone contribution increases from 61% in CESM2-CAM-Zender to 88% in CESM2-CAM-Kok, but slightly decreases from 63% in E3SM2-Zender to 58% in E3SM3-Kok. The three GISS-E2 models ~~show no differences in the regional distributions . However, the total emission is~~ produce consistent distributions across climate zones, although total emissions are about 40% lower when using the MATRIX aerosol scheme~~. This could be due to different model tuning parameters, or underestimation~~ , possibly due to parameter tunings or underrepresentation of coarse dust ~~particles~~ (>5 μm diameter) in the MATRIX modal size distribution ~~, as pointed out by Bauer et al. (2022).~~ (Bauer et al., 2022).

UKESM1.0 ~~simulates~~ emits nearly twice as much dust as HadGEM3-GC3.1, ~~along with slightly more even~~ and exhibits slightly more uniform spatial distributions. As described in Woodward et al. (2022), UKESM1.0 is built ~~on~~ upon HadGEM3-GC3.1 but applies ~~model~~ parameter tunings that enhance friction velocity and suppress soil moisture~~. These tunings are expected to increase~~ , effectively increasing the wind gustiness and soil ~~dryness~~ aridity leading to more emissions in UKESM1.0~~, thereby strengthening dust emissions. UKESM1.0 also excludes emissions from seasonally vegetated regions, resulting in smaller dust-emitting areas (Fig. 2p) compared to HadGEM3-GC3.1 (Fig. 2o).~~ . The three Japanese models (MRI-ESM2.0, MIROC-ES2L, and MIROC6) ~~exhibit large differences~~ also differ markedly in total emissions and, to a lesser ~~degree, regional~~ extent, spatial distributions. MRI-ESM2.0 produces similar regional fractions to JRAero but nearly ~~twice the total emissions~~doubles the total emission magnitude. Despite using the same dust ~~scheme~~parameterization, MIROC-ES2L ~~produces~~ emits roughly five times more dust than MIROC6. This discrepancy can be largely explained by ~~the~~ stronger winds in MIROC-ES2L, which produces 50% higher global mean wind speed than MIROC6. Moreover, MIROC6 prescribes non-zero LAI even in hyperarid

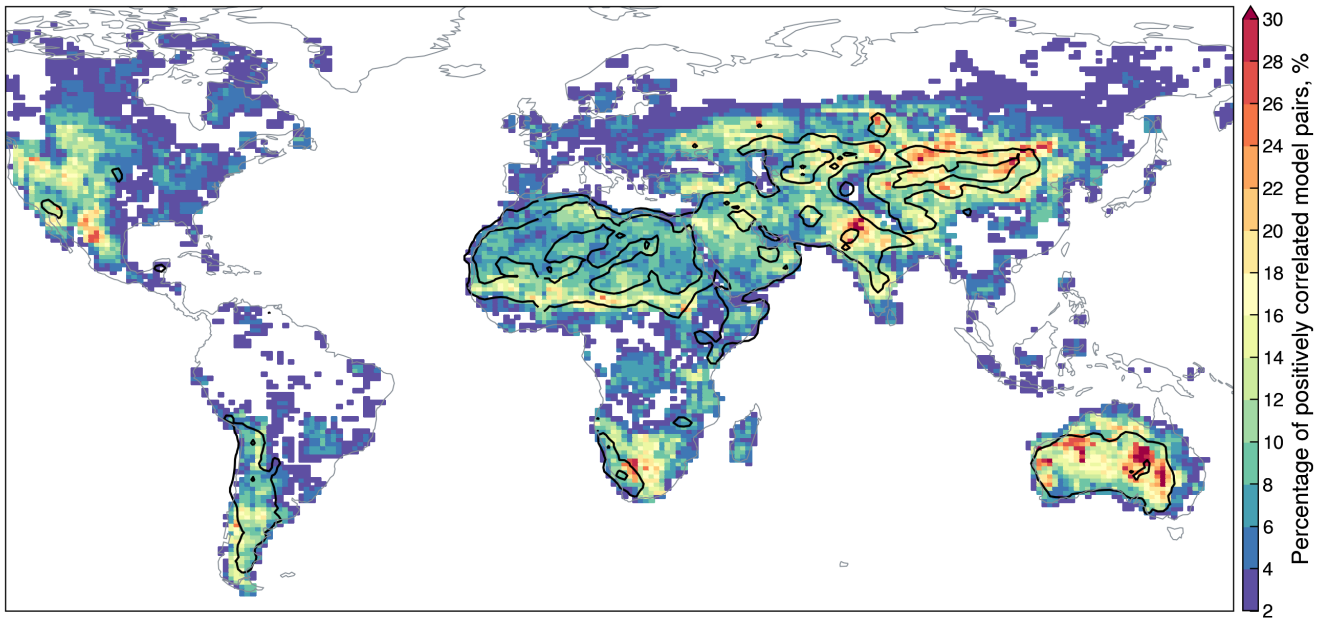

Figure 4. Percentage of statistically significant ($p \leq 0.1$), positive correlations out of every possible pairwise comparisons of deseasonalized monthly dust emission fluxes from 21 Earth system models. Black contours ~~represent~~ indicate the model ensemble mean ~~annual dust~~ emission flux of 10 and 100 Tg yr^{-1}.

~~regions, which likely further suppresses dust emissions~~ areas, likely further suppressing dust generation relative to MIROC-ES2L (Hiroaki Tatebe, personal communications).

Based on the model ensemble mean, global dust emissions are partitioned as 61% from hyperarid, 27% from arid, and 5% from semiarid zones. In comparison, MERRA2 and JRAero allocate the vast majority of dust emissions to hyperarid and arid zones, with negligible contributions from the semiarid zone.

3.2 Interannual variability

This section evaluates the consistency among the ESMs in simulating the interannual variability of dust emissions. Monthly dust emission fluxes from all ESMs are first regridded to a common resolution of 0.9°×1.25° (the native grid of CESM2). To remove the influence of annual cycles, ~~we subtract the~~ month-wise climatological means are subtracted from each grid cell, yielding deseasonalized dust emission flux anomalies. Spearman's rank correlation coefficients are then calculated between the ~~deseasonalized anomalies for all possible model pairs~~monthly anomalies for every possible model pair. With 21 ESMs, this ~~yields~~ results in 210 pairwise comparisons. To quantify ~~the extent of~~ inter-model agreement, we calculate the percentage of model pairs ~~that exhibit~~ exhibiting statistically significant ($p \leq 0.1$), positive correlations~~, which is displayed in Fig. 4.~~. A

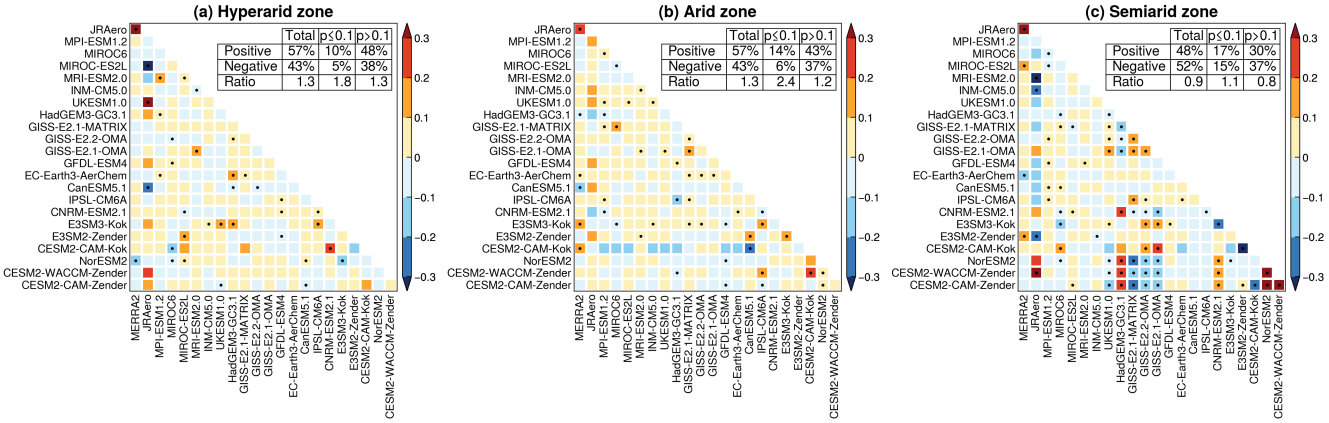

Figure 5. Spearman's rank correlation coefficients between dust emission flux anomalies averaged over hyperarid, arid, and semiarid climate zones. Dots indicate statistically significant correlations ($p \leq 0.1$). Summary tables are based on Earth system models only (MERRA2 and JRAero not included).

higher percentage indicates stronger inter-model agreement in simulating the ~~interannual variability of dust emissions.~~ dust variability, and vice versa. The results are displayed in Fig. 4.

Despite ~~its~~ the dominant contributions to global dust emissions, the hyperarid ~~zone shows generally poor model~~ climate zone exhibits generally poor inter-model agreement, with less than 10% of pairwise comparisons ~~yielding statistically significant~~ , showing statistically significant positive correlations. Because dust emissions from hyperarid areas are ~~primarily controlled by~~ predominantly controlled by near-surface wind speed, this ~~weak agreement reflects inconsistent wind simulations in~~ poor agreement reflects inconsistencies in wind simulations among the ESMs. Indeed, we find that only 10% of model pairs produce ~~statistically significant,~~ positively correlated wind variability~~in the hyperarid zone. Similarly,~~ . Evan (2018) reported that dust-producing winds over the Sahara Desert are mainly driven by large-scale meteorological processes and that most CMIP5 models failed to capture the near-surface wind variability. These results ~~suggest that accurately representing~~ indicate that improving the representation of near-surface winds is critical for reducing ~~model~~ inter-model discrepancies in dust variability over hyperarid ~~areas~~regions.

~~Compared~~ In contrast to the hyperarid zone, the arid and semiarid zones (such as the Sahel, South Asia, East Asia and Australia) exhibit significantly ~~stronger model~~ better agreement. To ~~illustrate~~ further assess how model consistency varies ~~with climate zones~~across climate regimes, Fig. 5 presents ~~the~~ pairwise correlation matrices based on dust emission flux anomalies averaged over hyperarid, arid, and semiarid zones. The percentage of statistically significant, positively correlated model pairs increases from 10% in the hyperarid zone to 14% in the arid zone and 17% in the semiarid zone, indicating progressively ~~higher model agreement in regions~~ better agreement where dust emissions are increasingly influenced by hydroclimate and land surface conditions. Meanwhile, the semiarid zone ~~exhibits~~ shows a larger percentage of negatively correlated model pairs (15%) ~~compared to~~ than the hyperarid (5%) and arid (6%) zones. This ~~dipole~~ dual pattern suggests that as the climate regime

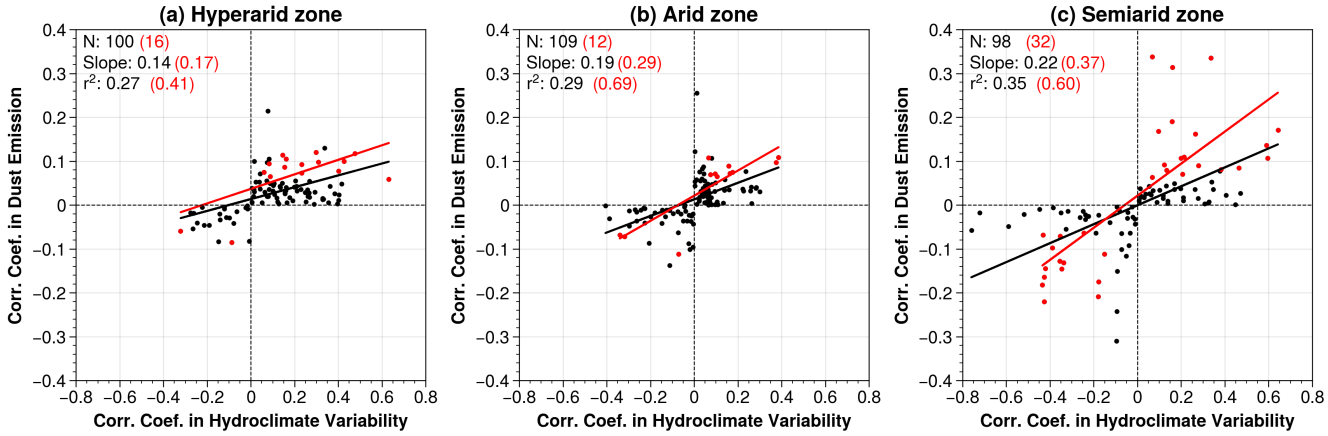

Figure 6. Statistical associations between ~~the~~ pairwise model correlation coefficients ($p \leq 0.1$ shown in red) in dust emission fluxes and hydroclimate variability over (a) hyperarid, (b) arid, and (c) semiarid climate zones.

transitions from hyperarid to semiarid, the ESMs exhibit both stronger agreement and ~~worsened~~ heightened disagreement in simulating ~~dust emission variability~~ the interannual variability of dust emissions.

~~What causes this complex behavior ? In semiarid environment~~ This behavior can be explained by the strong influence of antecedent land surface conditions on soil erodibility in semiarid environments such as temperate grasslands and steppes ~~, dust emissions are strongly modulated by antecedent land surface conditions in addition to wind speed,~~ (Shinoda et al., 2011; Nandintsetseg and . In these regions, factors such as precipitation, soil moisture, and vegetation ~~growth-decay cycle, which exert strong lagged influence on the soil erodibility (Shinoda et al., 2011; Nandintsetseg and Shinoda, 2015)~~growth–decay cycles have lagged and long-lasting impacts on the availability of erodible sediments. For example, dry anomalies during the ~~prior wet season (e.g., reduced snowfall or rainfall , accelerated snow retreat) can subsequently~~ wet season such as reduced rainfall or earlier snowmelt can decrease soil cohesion and suppress vegetation growth, thereby prolonging bare soil exposure and ~~increasing wind erosionrisk~~enhancing the risk of wind erosion. This delayed ~~dust emission response to preceding drought exemplifies the effect of~~ response exemplifies the land surface memory ~~, whereby~~ effect, in which the slow adjustment of ~~land surface states (such as soil moisture, snow cover, and vegetation)~~ soil and vegetation conditions over weeks to months influences subsequent dust ~~emission~~ emissions long after the initial hydroclimate forcing (e.g., drought). ~~Therefore, we speculate~~ We therefore hypothesize that the simultaneous increase ~~of both model consistency and divergence~~ in both model agreement and disagreement from hyperarid to semiarid zones reflects a ~~"~~“double-edged sword~~" ~~~~” effect of land surface memory: models with coherent representations of hydroclimate variability ~~converge in the simulated dust emission~~ tend to converge in simulated dust variability (i.e., more positive correlations), ~~while~~ whereas those with divergent hydroclimate representations diverge in the dust variability (i.e., more negative correlations).

To verify this hypothesis, we examine the statistical association between pairwise model correlations in dust emissions and those in hydroclimate variability. Specifically, we ~~first~~ perform a principle component analysis (PCA) of the five hydroclimate

variables (i.e., precipitation, soil moisture, specific humidity, air temperature, LAI) separately for the hyperarid, arid, and semiarid zones. The leading principle component (PC1), which explains at least 40% of the total variance in all zones, is used as a proxy for the dominant hydroclimate variability. Spearman's rank correlation coefficients are then ~~calculated~~ computed for all pairwise ~~model~~ comparisons of deseasonalized monthly PC1 values, following the same approach as in Fig. 5.

Figure 6 compares the correlation coefficients for model pairs with the same sign (i.e., ~~either~~ both positive or both negative) in dust emission fluxes and hydroclimate PC1. The regression slope and coefficient of determination (r^2) quantify the degree of statistical association between ~~model~~ inter-model correlations in dust emission and hydroclimate variability. The positive ~~association in~~ relationships across all climate zones suggests that ESMs with stronger consensus in hydroclimate variability also tend to produce more consistent dust variability, and vice versa. More importantly, both the number of significantly correlated model pairs (N) and correlation strength (slope and r^2) show significant increases from hyperarid to semiarid zones. This result supports our ~~hypothesis~~ speculation regarding the dual role of land surface memory: it enhances agreement among ESMs with coherent hydroclimate representations, while simultaneously ~~exacerbating~~ amplifying disagreement among those with divergent hydroclimate variability.

3.3 Relative importance of wind and hydroclimate drivers

In this section, we present ~~the dominance analysis of~~ dominance analysis results on the collective and relative influence of wind and hydroclimate drivers on the ~~dust emission variability~~ simulated dust variability within each model. Figure 7 ~~presents~~ shows the total variance explained (R^2) by ~~near-surface~~ wind speed and five hydroclimate ~~variables~~ drivers (precipitation, soil moisture, specific humidity, air temperature, and LAI) in the ESMs and MERRA2. Results for CESM2-WACCM-Zender and NorESM2 are very similar to those of CESM2-CAM-Zender and thus not shown.

The ESMs ~~exhibit substantial differences~~ show large discrepancies in the total R^2, reflecting ~~a large spread in the internal model variability and~~ inherent differences in the coupling strength between dust emission and ~~the six selected predictors. CanESM5.1 yields the lowest global~~ physical drivers. When ranked by the global mean R^2, CanESM5.1 shows the lowest explanatory power of the predictors, followed by MPI-ESM1.2, MIROC6, and EC-Earth3-AerChem~~, in which the selected predictors explain a relatively small fraction of the dust variability. The low explanatory power may~~. The weak predictor–response relationship can be explained by several ~~reasons. Specifically, model deficiencies and~~ factors. Model deficiencies or errors (e.g., in CanESM5.1, Section 3.1) ~~may~~ can weaken or distort the simulated relationships between dust ~~emissions and the predictors. The use of over-simplified~~ emission and physical drivers. Simplified parameterizations and/or static land surface input ~~(e.g., in INM-CM5.0) may weaken the dust–predictor relationship~~can reduce the dust sensitivity to hydroclimate conditions. In addition, ~~dust emission involves inherently nonlinear processes and thus its relationship with~~ because dust emission is governed by highly nonlinear threshold processes, its dependence on the predictors may deviate from the ~~linearity assumption in~~ linear assumptions underlying dominance analysis. As shown in Fig. 7, ~~the~~ total R^2 values ~~tend to be much~~ are generally lower in arid and semiarid ~~zones than in the hyperarid zone~~areas than in hyperarid areas, likely due to increased nonlinearity ~~between dust emission and hydroclimate variables which diminishes their collective explanatory power in a multilinear regression framework. Finally, the use of monthly model output, due to data availability, may dampen the short-term variability and~~

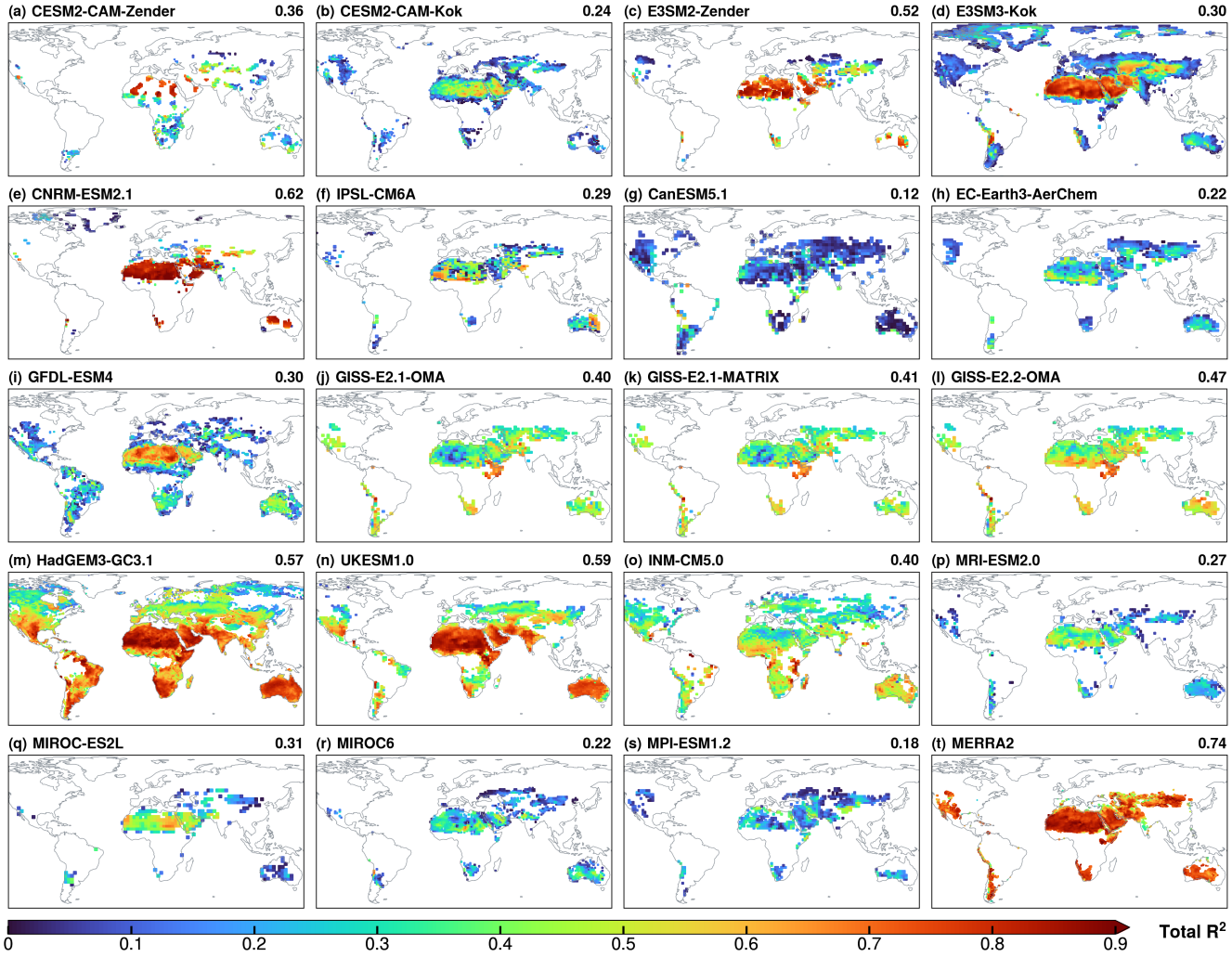

Figure 7. Total explained variance (R^2) in dust emission fluxes by six near-surface ~~predictors~~ variables (wind speed, precipitation, soil moisture, specific humidity, air temperature and LAI) in Earth system models and MERRA2. Global mean R^2 values are shown on each panel.

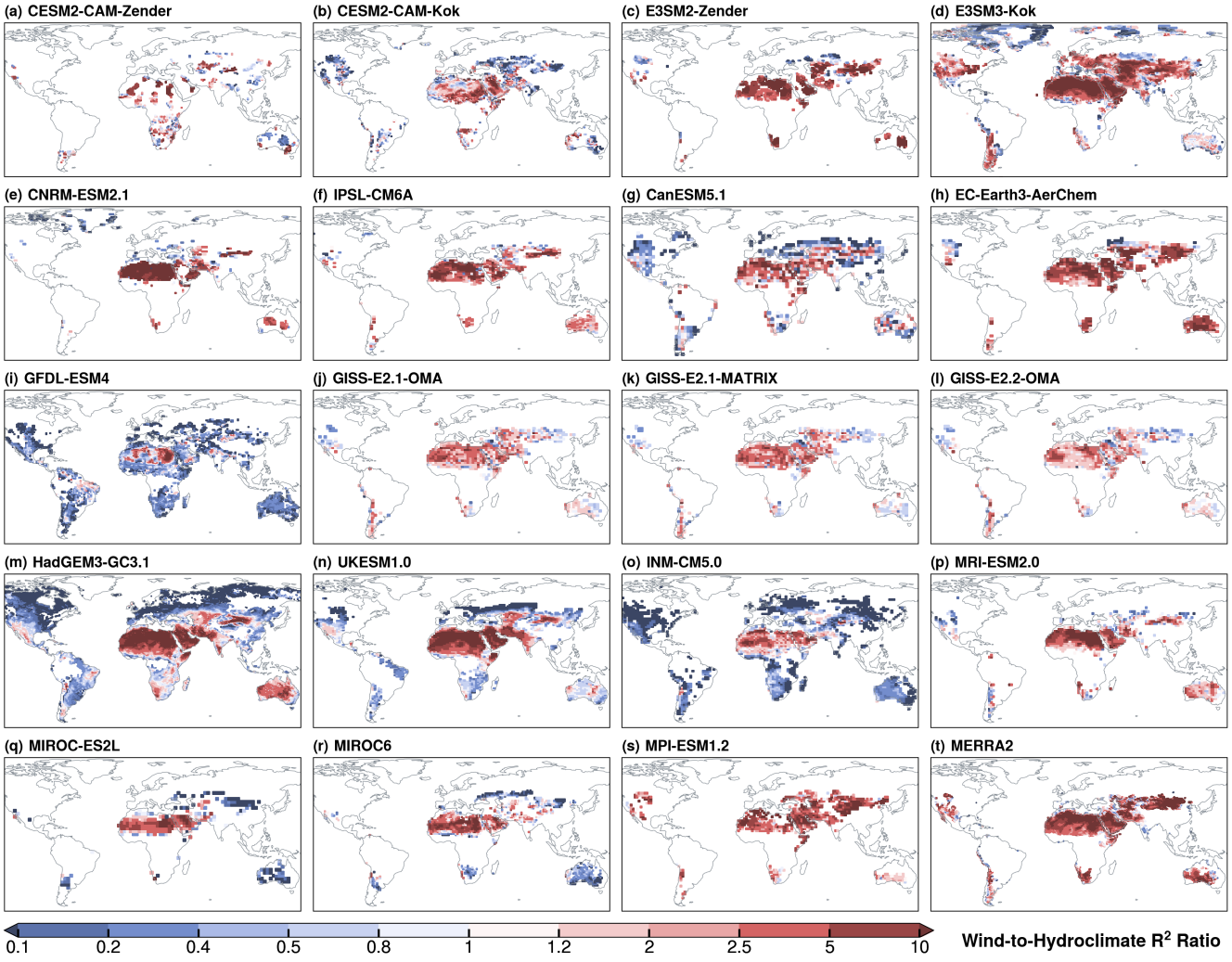

Figure 8. The ratio of wind speed-associated R^2 to the combined R^2 of five hydroclimate ~~variables~~ drivers (precipitation, soil moisture, specific humidity, air temperature and LAI) in Earth system models and MERRA2.

statistical association between dust emission and the predictors. in the dust-hydroclimate relationships that diminishes the explanatory power of multilinear regression models.

Despite these limitations, most ESMs produce significant total R^2 values over major source areasdust sources, especially in the hyperarid zone where the total hyperarid areas with R^2 exceeds 0.6above 0.5. Switching from the Zender to Kok dust scheme leads to generally lower generally reduces R^2 values in in both CESM and E3SM (Fig. 7a–d). The GISS-E2 models show little differences between the OMA or MATRIX schemes, and and MATRIX aerosol schemes, with a modest increase from version 2.1 to 2.2. UKESM1.0 and HadGEM3-GC3.1 show minimal differences, both with showing high R^2 values globally. MIROC6 yields lower R^2 than MIROC-ES2L, especially over the hyperarid zoneparticularly over hyperarid areas. MERRA2 produces higher R^2 than most ESMs, especially over within arid and semiarid zones. In summary, there are large spatial variability within individual ESMs and large inter-model discrepancies in the variance explained by the , indicating a stronger overall coupling between dust emissions and the selected predictors.

To assess the relative importance of wind and hydroclimate drivers, Fig. 8 displays presents the ratio of the wind speed-associated R^2 to the combined R^2 of the five hydroclimate variables. In all ESMs except GFDL-ESM4, the this wind-to-hydroclimate R^2 ratio is well above 1 over the hyperarid zone, which is hyperarid areas, consistent with the dominant role control of wind speed in controlling dust emissions on dust emission from persistently dry, barren surfaces. In contrast, arid and semiarid zones exhibit greater areas exhibit greater inter-model discrepancies, with ratios either above or below 1 depending on the model. This reflects increased model discrepancies regarding the relative importance of wind and substantial uncertainty in how models represent the relative influence of wind versus hydroclimate drivers in transitional regions where dust emission is increasingly influenced by regions where hydroclimate and land surface conditions exert strong effects on sediment availability.

Based on the wind-to-hydroclimate R^2 ratios, we classify global dust-emitting areas into three regimes: wind-dominated (ratio$>$1.2), hydroclimate-dominated (ratio$<$0.8), and equally-important (0.8–1.2). We then Then we calculate the fractions of dust emissions originating from the three regimes in emitted from these regimes within each model. The results are displayed in Fig. 9. The ESMs show general agreement in the "equally-important" regime, with most models producing simulating less than 10% of dust from regions where wind and hydroclimate drivers have nearly equal influenceon dust emissions. GFDL-ESM4 produces the highest contribution (12%) in this regime.

The wind-dominated regime contributes accounts for the majority of global dust emissions (>80%) in most ESMsand MERRA2, consistent with the dominant contribution of the hyperarid zone from hyperarid areas (Fig. 3). However, three models yield anomalously low contributionsestimates: GFDL-ESM4 (36%), INM-CM5.0 (5443%) and CanESM5.1 (75%). These deviations can be explained by different reasons. As shown in Fig. 3, INM-CM5.0 and CanESM5.1 produce relatively spatially homogeneous emission pattern, which explains the lower contributions homogeneous emission patterns, which reduce the fractional contribution from hyperarid or wind-dominated areas. In comparisonregions. In contrast, the low estimate in GFDL-ESM4 is due to the model's results from its anomalously strong hydroclimate influence over the hyperarid zonehyperarid areas. As shown in Fig. 8i, GFDL-ESM4 exhibits yields markedly low wind-to-hydroclimate ratios ($<$1) over North Africa, Arabian Peninsula, and Iranian Plateau, which are consequently misclassified into the leading to the misclassification of these inherently wind-dominated regions as hydroclimate-dominatedregime. These regions are characterized by scarce precipitation and very

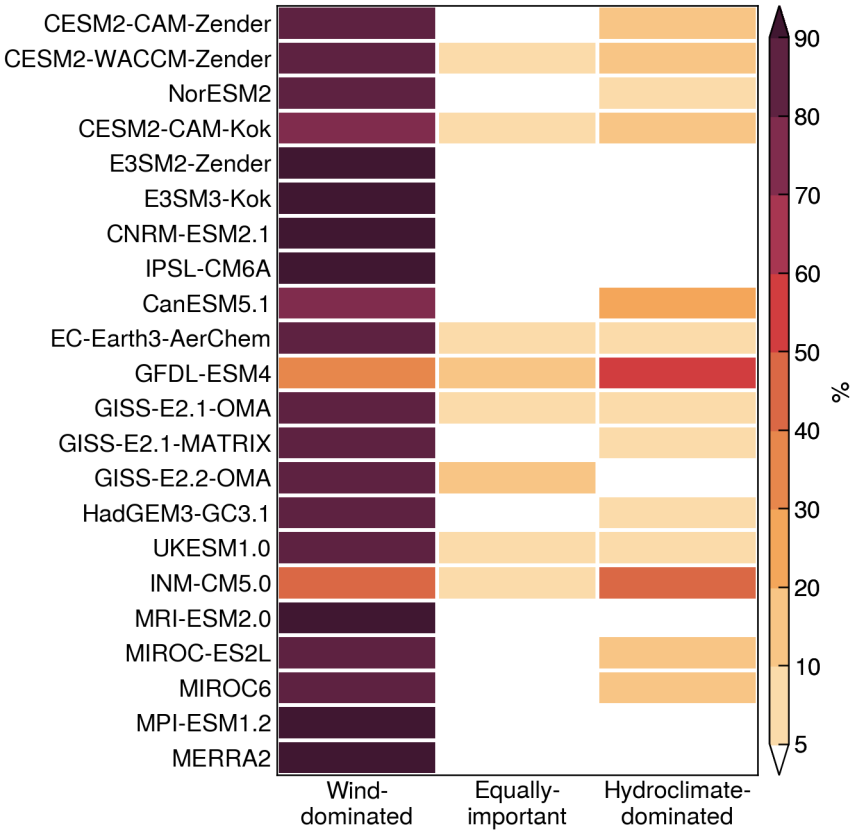

Figure 9. Fractional contributions of wind-dominated, equally-important, and hydroclimate-dominated regimes to global dust emissions in Earth system models and MERRA2.

. Given the extremely scare precipitation and low hydroclimate variability ~~, which is expected to have negligible influence on dust emissions.~~ in these regions, such strong hydroclimate influence is likely unrealistic and points to possible deficiencies in the model.

For CESM and E3SM, switching from the Zender to Kok dust scheme slightly reduces the wind-dominated dust fraction: from 85% to ~~80~~79% in CESM, and from 99% to 96% in E3SM. The GISS-E2 models yield similar ~~estimates~~ results regardless of model version or aerosol scheme, with ~~82–85~~87–90% dust from the wind-dominated regime. ~~Similarly~~Likewise, UKESM1.0 and HadGEM3-GC3.1 yield ~~similar~~ nearly identical estimates, with 90% of dust ~~emitted~~ from wind-dominated regions. MERRA2 simulates 98% emissions from ~~the~~ wind-dominated ~~regime~~areas, higher than most ESMs.

The above analysis not only confirms the anomalous dust emission patterns in CanESM5.1 and INM-CM5.0 ~~as previously~~ (shown in Fig. 3), but also identifies GFDL-ESM4 as an outlier due to its misrepresentation of ~~predictor relative importance~~ the relative importance of wind and hydroclimate drivers. Here we further ~~evaluate the contribution of wind speed~~ examine the wind speed fractional contributions to the total R^2 ~~in~~ across different climate zones. For each ~~climate~~ zone, we use ridgeline

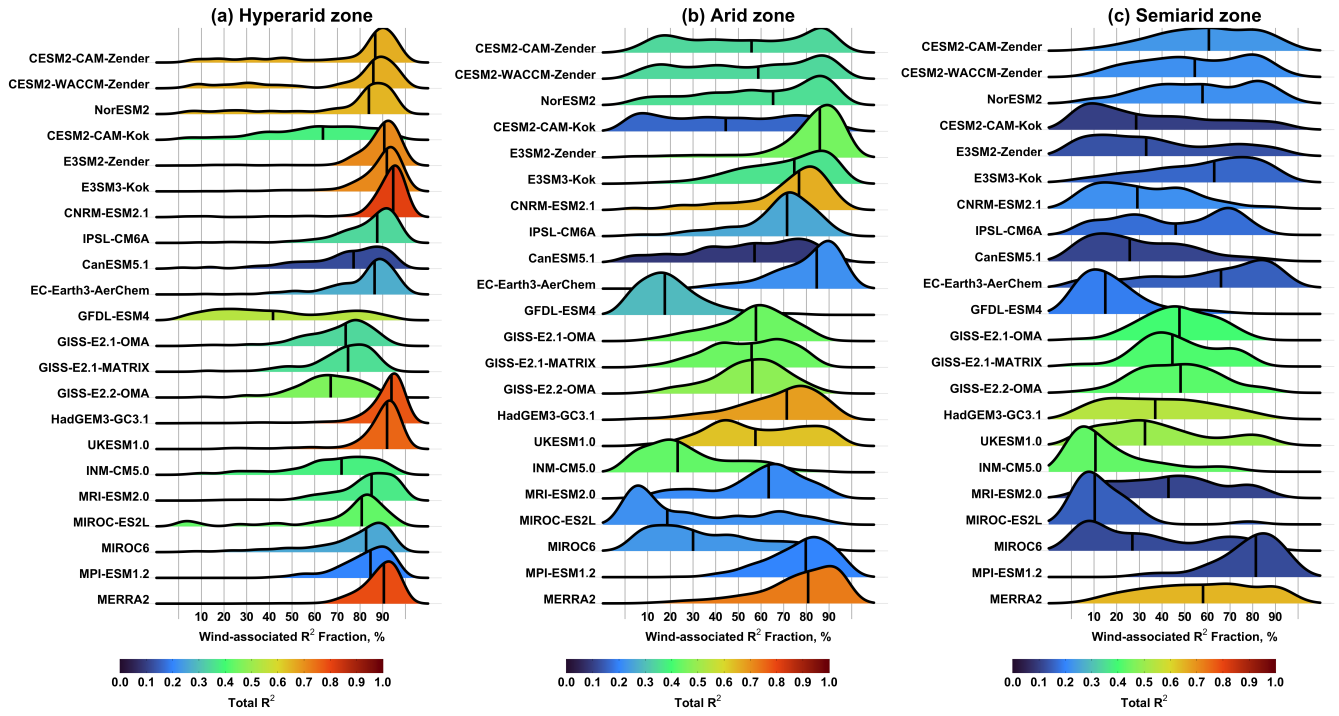

Figure 10. Ridgeline plots of the fractional contributions of wind speed to the total R^2 over (a) hyperarid, (b) arid, and (c) semiarid climate zones. ~~The median and mean values are denoted by red and blue~~ Black vertical lines ~~, respectively~~indicate median values. Color shading represent the mean total R^2 values.

plots to illustrate the statistical distributions of grid-level ~~wind speed-associated~~ wind-associated R^2 fractions. The results are displayed in Fig. 10. In ~~the ridgeline plots, if the median value of wind speed-associated~~ these plots, the black vertical lines indicate the median values. When the median wind-associated R^2 ~~fractions (denoted by a red vertical line in Fig. 10)~~ fraction is above 50%, ~~it means wind speed dominates the dust variability at~~ more than half of the grid cells ~~. If the median value is~~ within the climate zone are dominated by near-surface winds in the dust variability. Conversely, when the median falls below 50%, ~~the dust variability is dominated by hydroclimate drivers at more than half of the grid cells~~hydroclimate drivers exert dominant control over the majority of the climate zone.

In the hyperarid zone (Fig. 10a), most ESMs ~~and MERRA2~~ capture the dominant control of wind speed, with ~~the median~~ median wind-associated R^2 fractions exceeding 80%. The three GISS-E2 models ~~show~~ display similar spatial variability, albeit with slightly lower ~~median values (~70~~wind contributions (67–74%). Two models stand out as ~~notable~~ outliers: GFDL-ESM4 and CESM2-CAM-Kok, both ~~of which exhibit large variability and low median values. In particular~~exhibiting great spatial variability and anomalously low wind influence, indicating an overestimation of hydroclimate influence over permanently dry, barren regions. Specifically, GFDL-ESM4 yields a median ~~wind~~ wind-associated R^2 fraction of 42%, ~~indicating an overestimated sensitivity to hydroclimate drivers in the hyperarid zone, particularly over~~ due to excessively strong hydroclimate

influence across North Africa, Arabian Peninsula, and Iranian Plateau (see Fig. 8i). Similarly, CESM2-CAM-Kok ~~exhibits large spatial variability with a median wind R^2 fraction~~ yields a median of 64%, ~~driven by~~ due to dominant hydroclimate influence over West Africa and the Tarim Basin (see Fig. 8b). In ~~comparison~~contrast, CESM2-CAM-Zender captures the ~~dominant wind influence~~ expected wind dominance with a median ~~value of 86~~of 87%. The ~~suboptimal performance of~~ overestimated hydroclimate influence in CESM2-CAM-Kok relative to CESM2-CAM-Zender persists ~~when comparing common dust-producing~~ even when compared over common dust-emitting areas in the ~~two~~ models.

In the arid zone (Fig. 10b), the total R^2 ~~is generally smaller due to~~ values are generally lower, reflecting reduced explanatory power of the selected predictors. The ESMs also ~~show larger disagreement~~ exhibit greater discrepancies in the relative importance of wind and hydroclimate drivers. ~~The influence of wind speed~~ Although the wind influence is reduced and more variable ~~, but still~~ than in the hyperarid zone, it remains dominant in most ESMs~~and MERRA2~~. The GISS-E2 models ~~produce relatively equal importance of~~ simulate nearly equal wind and hydroclimate ~~drivers. In contrast, four~~ influences. Four models—GFDL-ESM4, INM-CM5.0, MIROC-ES2L and ~~MIROC6—yield dominant hydroclimate influence with the median wind~~ MIROC6—exhibit median wind-associated R^2 ~~fraction falling~~ fractions well below 50%, ~~indicating~~ signifying a transition from wind- to hydroclimate-dominated regimes. CESM2-CAM-Kok also reflects this transition, although to a small extent with a median ~~value~~ of 46%. In both CESM and E3SM, ~~switching from the Zender to Kok scheme results in weaker wind and stronger hydroclimate influences, likely due to the~~ replacing the Zender with Kok dust scheme weakens the wind influence while strengthening the hydroclimate influence, with the median wind-associated R^2 fraction declining from 56% to 44% in CESM and from 86% to 74%. This is consistent with previous findings that physically based soil erodibility ~~treatment~~ formulations in the Kok scheme ~~which enhances~~ enhance the dust sensitivity to ~~hydroclimate variability , as previously suggested in~~ climate variability Kok et al. (2014a).

Results for the semiarid zone (Fig. 10c) are ~~considered~~ less robust due to significantly smaller dust-emitting areas or ~~model~~ grid cells (see Fig. 1). ~~In general, the wind influence further declines~~Overall, the influence of wind speed further weakens, while hydroclimate ~~divers~~ drivers become more important. The magnitude of this shift, however, varies ~~widely, leading to larger discrepancies~~considerably among ESMs. Specifically, ~~hydroclimate drivers continue to dominate~~ only three models (E3SM3-Kok, EC-Earth3-AerChem and MPI-ESM1.2) retain the wind dominance, albeit with greater spatial variability. Hydroclimate dominance persists in CESM2-CAM-Kok, GFDL-ESM4, INM-CM5.0, MIROC-ES2L and MIROC6, ~~same as~~ consistent with their behaviors in the arid ~~zone. The following ESMs display a clear transition~~ climate zone. In contrast, multiple models display a transition from wind- to hydroclimate-dominated regimes: E3SM2-Zender, CNRM-ESM2.1, CanESM5.1, HadGEM3-GC3.1, and UKESM1.0. ~~IPSL-CM6A and~~ The GISS-E2 models ~~also show increased~~ and IPSL-CM6A exhibit moderate increases of hydroclimate influence, ~~though to a lesser extent. The remaining ESMs~~and resulting in roughly equal importance of wind and hydroclimate drivers. Compared to the ESMs, MERRA2 ~~continue to display dominance of wind speed, albeit with increased spatial variability~~generally produces dominant wind influence across all three climate zones.

The above analysis indicates that GFDL-ESM4 and CESM2-CAM-Kok simulate anomalously strong hydroclimate ~~influence in~~ influences within the hyperarid zone. To ~~identify the specific drivers~~ diagnose the sources of these anomalies, Fig. 11 presents the median fractional contributions of five hydroclimate variables to the total R^2. In the hyperarid zone, most ESMs capture

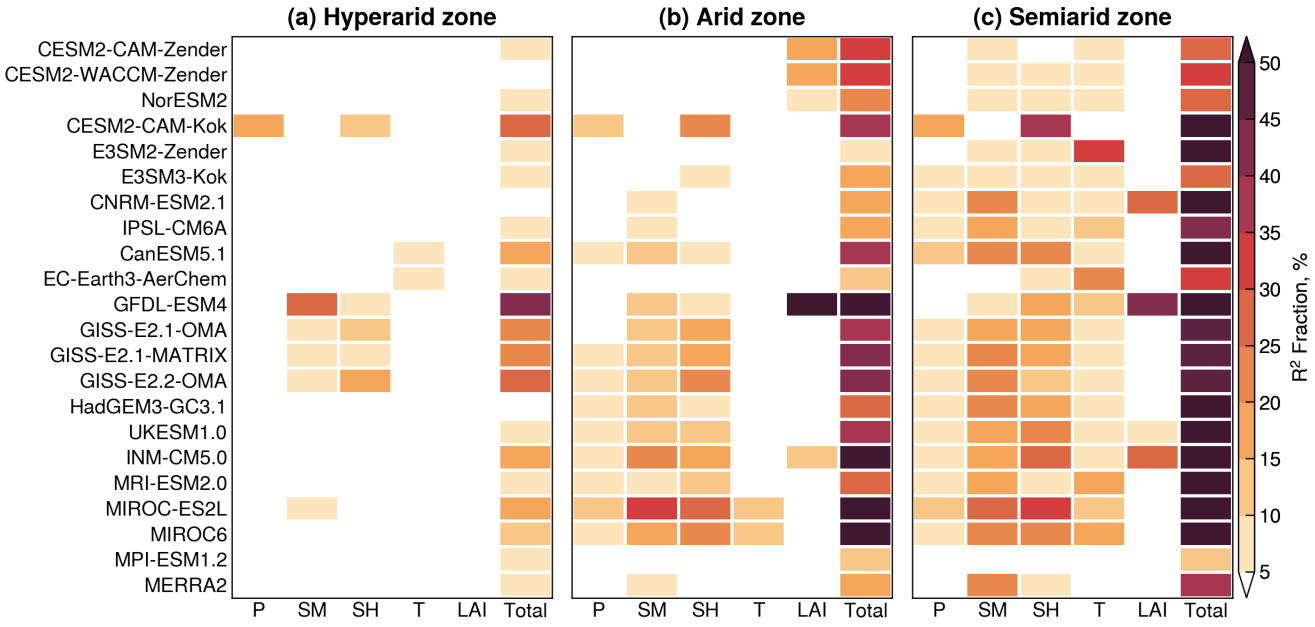

Figure 11. Median factional contributions of hydroclimate ~~variables~~ drivers to the total explained variance (R^2) in Earth system models and MERRA2 over (a) hyperarid, (b) arid, and (c) semiarid climate zones. Hydroclimate variables are precipitation (P), soil moisture (SM), specific humidity (SH), air temperature (T), and leaf area index (LAI).

the ~~negligible sensitivity of dust emission to hydroclimate variables. Several exceptions exist, however. CESM2-CAM-Kok shows unusually strong influence from precipitation and specific humidity, while~~ expected negligible influence of hydroclimate drivers. GFDL-ESM4 ~~exhibits anomalously strong sensitivity to soil moisture~~and CESM2-CAM-Kok stand out as outliers, producing anomalously high influence from soil moisture and precipitation, respectively. The influence attributed to specific humidity can be interpreted as a soil moisture effect, given the close coupling between surface soil water content and near-surface humidity through evapotranspiration. The GISS-E2 models ~~display moderately elevated sensitivity to~~ also display elevated contributions from soil moisture and specific humidity, which explains their ~~moderate~~ modest wind influence in the hyperarid zone~~(~~, as shown in Fig. 10a~~)~~.

The ~~overestimation of~~ anomalous hydroclimate influence in the hyperarid zone ~~may~~ can be explained by ~~a combination of two~~ two possible mechanisms: (1) the ~~hydroclimate variability is overestimated in the model, which induces~~ model overestimates the hydroclimate variability, leading to spurious effects on dust emissions; or (2) the ~~hydroclimate variability is reasonably captured, but the dust scheme incorporates overly strong~~ model reasonably represents the hydroclimate variability but overestimates the dust sensitivity to hydroclimate drivers. For example, Shevliakova et al. (2024) reported that the GFDL-ESM4 land model significantly overestimates surface soil moisture over ~~dryland regions, with values more than double those from satellite observationsin dust source regions like the central Sahara and Tarim Basin~~major dust source areas, by as much as a factor

of two compared to satellite observations. This bias likely explains the ~~strong apparent sensitivity of dust emission to soil moisture~~ unrealistically large soil moisture influence on dust emissions in GFDL-ESM4~~(Fig. 11a).~~ .

The ~~abnormal~~ anomalous hydroclimate influence in CESM2-CAM-Kok may be partly ~~explained by~~ due to dust emission parameterizations in the Kok scheme ~~,~~ which introduces enhanced sensitivity to ~~the threshold wind velocity compared to~~ soil moisture compared with the Zender scheme (Kok et al., 2014a). ~~Because of this heightened dependence on land surface conditions, the Kok scheme does not require predefined dust source functions and is considered more physically realistic for projecting dust responses to future climate and land-use changes.~~ Another possible reason is the ~~relatively~~ short simulation period ~~in~~ for CESM2-CAM-Kok (2004–2013), which may ~~not fully capture the long-term~~ be insufficient to capture the full range of dust variability and predictor ~~influence as in~~ relationships relative to CESM2-CAM-Zender (1980–2014). In this regard, the E3SM experiments provide a more robust comparison between the ~~Zender and Kok~~ two dust schemes. As shown in Fig. 11a, ~~the E3SM models~~ both E3SM2-Zender and E3SM3-Kok exhibit negligible hydroclimate influence in the hyperarid zone~~, regardless of the dust scheme used~~. In the arid zone, however, E3SM3-Kok ~~shows higher~~ exhibits stronger hydroclimate influence than E3SM2-Zender~~due to increased sensitivity to specific humidity (Fig. 11b). This comparison provides additional~~ , providing new evidence that the Kok scheme amplifies the dust emission sensitivity to hydroclimate conditions compared to the Zender scheme, as previously suggested by Kok et al. (2014a).

In the arid zone (Fig. 11b), ~~most ESMs show enhanced influence from~~ the enhanced hydroclimate influence is primarily attributed to soil moisture and specific humidity in most ESMs, consistent with ~~empirical evidence that both variables strongly affect the soil erodibility and wind erosion risk (e.g., Csavina et al., 2014; RAVI et al., 2006; Kim and Choi, 2015). Interpreting the LAI influence, however, is more complex due to several factors. First, unlike~~ their well-established role in modulating soil erodibility (e.g., Csavina et al., 2014; RAVI et al., 2006; Kim and Choi, 2015). Several models—including CESM, GFDL-ESM4 and INM-CM5.0—assign strong influence to LAI. Unlike other hydroclimate variables, LAI ~~can~~ may be either prescribed from climatology or ~~simulated by the model's dynamic vegetation component~~ interactively simulated in models coupled with dynamic vegetation components, such as CESM and GFDL-ESM4 (Table 1). Models using prescribed LAI are ~~expected to show minimal~~ likely to show limited interannual variability and ~~hence limited~~ minimal influence on dust emissions. ~~Second~~For CESM and GFDL-ESM4, the LAI ~~effect on dust emission is treated differently. For example, CESM assumes a linear relationship between~~ influence reflects the vegetation effect on bare soil fraction~~and LAI when LAI is below 0.3, while GFDL-ESM4 assumes an exponential decrease in bare soil fraction as a function of LAI. Because LAI is often used to derive bare soil fraction~~ , a key parameter in vertical dust flux calculations~~, these differences can alter the modeled dust sensitivity to vegetation cover. Most ESMs in Fig. 11b exhibit weak to negligible LAI influence, likely reflecting either prescribed LAI or the normalization of dust fluxes prior to dominance analysis (see Section 2). One outlier is~~ . Specifically, bare soil fraction is calculated from LAI assuming a linear relationship in CESM and an exponential relationship in GFDL-ESM4~~which exhibits the strongest sensitivity to LAI , even well above the sensitivity to soil moisture. This can be explained by the strong coupled between LAI and dust emission in the model, and the fact that no normalization was applied to GFDL-ESM4 due to missing bare soil fraction output from the CMIP6 archive~~.

4 Conclusions

This study evaluates discrepancies ~~and biases~~ among 21 ESMs in representing the interannual variability of windblown dust emissions and the relative importance of near-surface wind speed and ~~hydroclimate drivers~~ five hydroclimate variables (precipitation, soil moisture, specific humidity, air temperature, and LAI) ~~. We treat~~ in modulating the dust variability. Treating dust emission flux as an unobservable, model-specific quantity~~and use~~ , we apply dominance analysis to quantify the ~~variance explained in dust emission fluxes by wind and hydroclimate~~ relative influences of physical drivers within each model~~. The analysis is conducted over three climatologically defined~~ , and compare the model behaviors across three climatologically-defined climate zones (hyperarid, arid, and semiarid)~~, and further examines the effect of dust emission parameterizations through paired CESM and E3SM experiments with the Zender et al. (2003) and Kok et al. (2014b) schemes~~.

The ~~hyperarid zone contributes more than half of global dust emissions in all models except CanESM5.1 and INM-CM5.0, which simulate relatively spatially even emission patterns with less than 50% from the hyperarid zone, likely due to known deficiencies and over-simplifications in dust emission representations~~extent of inter-model agreement in simulated dust variability exhibits a strong dependence on climate aridity. In the hyperarid zone, the ESMs ~~exhibit poor agreementwith each other and with MERRA2 in simulating the dust variability~~show poor agreement, with only 10% ~~of pairwise model~~ out of 210 pairwise comparisons yielding statistically significant, positive correlations. This poor agreement largely reflects inconsistencies in simulated near-surface winds. In arid and semiarid zones, the ESMs exhibit a ~~dipole pattern with both improved agreement and increased disagreement. This behavior can be explained~~ dual pattern driven by a "double-edged sword" effect of land surface memory: models with coherent representations of hydroclimate variability tend to converge in their simulated dust variability, ~~while~~ whereas those with divergent hydroclimate representations diverge in dust emission responses.

The relative ~~influence~~ importance of wind and hydroclimate drivers also varies with climate ~~regimes. Most~~ aridity. In the hyperarid zone, most ESMs capture the ~~dominant control of wind speed and weak sensitivity to hydroclimate conditions in the hyperarid zone~~expected dominant wind control and minimal hydroclimate influence, except CESM2-CAM-Kok and GFDL-ESM4, ~~both of which show great spatial variability and abnormally strong influence from precipitation , specific humidity,~~ which show unusually strong sensitivities to precipitation and soil moisture. The overestimated hydroclimate influence in GFDL-ESM4 can be explained by the model's overestimation of soil moisture in drylands and consequent spurious effects on dust emissions. The ~~enhanced~~ overestimated hydroclimate influence in CESM2-CAM-Kok ~~(relative to CESM2-CAM-Zender) may be explained, at least partly ,~~ may be partly explained by the physically based soil erodibility ~~formulations~~ formulation in the Kok et al. (2014b) ~~scheme, which replaces the use of predefined dust source functions~~dust scheme. A similar pattern is found in E3SM, where ~~switching from the Zender et al. (2003) to~~ replacing the Zender et al. (2003) scheme with the Kok et al. (2014b) scheme ~~strengthens the hydroclimate influence~~ enhances the hydroclimate contribution to dust variability in the arid zone. ~~However, due to concurrent updates in model physics (e.g., dust mineralogy , radiative feedbacks, and meteorology), further~~ Due to compounding factors such as model physics and dust mineralogy treatments in CESM and E3SM, however, additional experiments are needed to ~~isolate~~ disentangle the effects of dust emission parameterizations on ~~dust–climate sensitivities~~ the simulated sensitivities to physical drivers.

In arid and semiarid zones, the ~~influence of wind speed~~ wind influence generally weakens while the hydroclimate influence strengthens ~~. However,~~ in all ESMs. But the relative importance of ~~wind and hydroclimate~~ these drivers becomes increasingly inconsistent~~between the models, with an increasing number of ESMs shifting toward comparable or dominant-dominated regimes. In general~~, with contrasting model behaviors in either retaining wind dominance or shifting toward hydroclimate dominance or near-equal importance between the two. Compared to the ESMs, MERRA2 ~~produces~~ generally produce stronger wind influence and weaker hydroclimate influence ~~than the ESMs~~across all three climate zones.

~~In summary~~Overall, this study provides new insights into how current ESMs represent the ~~temporal~~ interannual variability and physical drivers of windblown dust emissions. ~~Most ESMs capture the dominant wind control over permanently dry, barren surfaces, their poor agreement in dust variability highlights large inconsistencies in the simulated~~ Our findings underscore that reducing model uncertainties in dust emission simulations requires (1) improved representations of near-surface ~~winds. The dipole model behavior in arid and semiarid zones underscores the important role of hydroclimate variability and land surface processes . Improving model representations of soil and vegetation dynamics and dust-climate interactions in these regions is essential for reducing uncertainties in future projections of dust emissions under changing climate and land-use conditions~~wind variability and gustiness in hyperarid regions, and (2) more accurate treatment of hydroclimate and land-surface processes in arid and semiarid regions.

Data availability. Model comparison and dominance analysis results are available at https://doi.org/10.5281/zenodo.15741734.

Author contributions. XX designed this study with input from LL. XX and XL performed the analysis and wrote the initial manuscript. LL performed CESM2-CAM-Kok simulations. YF performed E3SM simulations. All authors edited the manuscript.

Competing interests. The authors declare no competing interests.

Acknowledgements. X.L. and X.X. are partially supported by the NASA Land-Cover and Land-Use Change Program. Y.F. acknowledges the support of the Energy Exascale Earth System Model (E3SM) project, funded by the U.S. Department of Energy (DOE), Office of Science, Office of Biological and Environmental Research. The work at Argonne National Laboratory was supported by the U.S. DOE Office of Science under contract DE-AC02-06CH11357. L.L. acknowledges support from the U.S. Department of Energy (DOE) under award DE-SC0021302, and from the Earth Surface Mineral Dust Source Investigation (EMIT), a National Aeronautics and Space Administration (NASA) Earth Ventures-Instrument (EVI-4) mission. He also acknowledges the high-performance computing resources provided by Derecho at the National Center for Atmospheric Research (NCAR), through NCAR's Computational and Information Systems Laboratory (CISL), which is sponsored by the National Science Foundation (NSF). The authors acknowledge the World Climate Research Programme for coordinating and promoting CMIP6, and thank the climate modeling groups for producing and making available their model output, the

Earth System Grid Federation (ESGF) for archiving the data and providing access, and the multiple funding agencies who support CMIP6 and ESGF.

References

Albani, S., Mahowald, N. M., Perry, A. T., Scanza, R. A., Zender, C. S., Heavens, N. G., Maggi, V., Kok, J. F., and Otto-Bliesner, B. L.: Improved dust representation in the Community Atmosphere Model, Journal of Advances in Modeling Earth Systems, 6, 541–570, https://doi.org/10.1002/2013MS000279, 2015.

Aryal, Y. and Evans, S.: Dust emission response to precipitation and temperature anomalies under different climatic conditions, Science of the Total Environment, 874, https://doi.org/10.1016/j.scitotenv.2023.162335, 2023.

Aryal, Y. N. and Evans, S.: Global Dust Variability Explained by Drought Sensitivity in CMIP6 Models, Journal of Geophysical Research: Earth Surface, 126, https://doi.org/10.1029/2021JF006073, 2021.

Azen, R. and Budescu, D. V.: The Dominance Analysis Approach for Comparing Predictors in Multiple Regression, Psychological Methods, 8, 129–148, https://doi.org/10.1037/1082-989X.8.2.129, 2003.

Balkanski, Y., Schulz, M., Claquin, T., Moulin, C., and Ginoux, P.: Global Emissions of Mineral Aerosol: Formulation and Validation using Satellite Imagery, in: Emissions of Atmospheric Trace Compounds, edited by Granier, C., Artaxo, P., and Reeves, C. E., pp. 239–267, Springer, https://doi.org/10.1007/978-1-4020-2167-1_6, 2004.

Bauer, S. E., Tsigaridis, K., Faluvegi, G., Nazarenko, L., Miller, R. L., Kelley, M., and Schmidt, G.: The Turning Point of the Aerosol Era, Journal of Advances in Modeling Earth Systems, 14, https://doi.org/10.1029/2022MS003070, 2022.

Bergametti, G., Marticorena, B., Rajot, J. L., Chatenet, B., Féron, A., Gaimoz, C., Siour, G., Coulibaly, M., Koné, I., Maman, A., and Zakou, A.: Dust Uplift Potential in the Central Sahel: An Analysis Based on 10 years of Meteorological Measurements at High Temporal Resolution, Journal of Geophysical Research: Atmospheres, 122, 433–12, https://doi.org/10.1002/2017JD027471, 2017.

Bryant, R. G.: Recent advances in our understanding of dust source emission processes, Progress in Physical Geography, 37, 397–421, https://doi.org/10.1177/0309133313479391, 2013.

Budescu, D. V.: Dominance analysis: A new approach to the problem of relative importance of predictors in multiple regression, Psychological Bulletin, 114, 542–551, https://doi.org/10.1037/0033-2909.114.3.542, 1993.

Bullard, J. E., Harrison, S. P., Baddock, M. C., Drake, N., Gill, T. E., McTainsh, G., and Sun, Y.: Preferential dust sources: A geomorphological classification designed for use in global dust-cycle models, Journal of Geophysical Research: Earth Surface, 116, https://doi.org/10.1029/2011JF002061, 2011.

Cakmur, R. V., Miller, R. L., and Torres, O.: Incorporating the effect of small-scale circulations upon dust emission in an atmospheric general circulation model, Journal of Geophysical Research: Atmospheres, 109, https://doi.org/10.1029/2003jd004067, 2004.

Cheng, T., Peng, Y., Feichter, J., and Tegen, I.: An improvement on the dust emission scheme in the global aerosol-climate model ECHAM5-HAM, Atmospheric Chemistry and Physics, 8, 1105–1117, https://doi.org/10.5194/acp-8-1105-2008, 2008.

Cowie, S. M., Marsham, J. H., and Knippertz, P.: The importance of rare, high-wind events for dust uplift in northern Africa, Geophysical Research Letters, 42, 8208–8215, https://doi.org/10.1002/2015GL065819, 2015.

Csavina, J., Field, J., Félix, O., Corral-Avitia, A. Y., Sáez, A. E., and Betterton, E. A.: Effect of wind speed and relative humidity on atmospheric dust concentrations in semi-arid climates, Science of the Total Environment, 487, 82–90, https://doi.org/10.1016/j.scitotenv.2014.03.138, 2014.

Engelstaedter, S., Kohfeld, K. E., Tegen, I., and Harrison, S. P.: Controls of dust emissions by vegetation and topographic depressions: An evaluation using dust storm frequency data, Geophysical Research Letters, 30, https://doi.org/10.1029/2002GL016471, 2003.

Evan, A. T.: Surface Winds and Dust Biases in Climate Models, Geophysical Research Letters, 45, 1079–1085, https://doi.org/10.1002/2017GL076353, 2018.

Evan, A. T., Flamant, C., Fiedler, S., and Doherty, O.: An analysis of aeolian dust in climate models, Geophysical Research Letters, 41, 5996–6001, https://doi.org/10.1002/2014GL060545, 2014.

Evans, S., Ginoux, P., Malyshev, S., and Shevliakova, E.: Climate-vegetation interaction and amplification of Australian dust variability, Geophysical Research Letters, 43, 823–11, https://doi.org/10.1002/2016GL071016, 2016.

Fécan, F., Marticorena, B., and Bergametti, G.: Parametrization of the increase of the aeolian erosion threshold wind friction velocity due to soil moisture for arid and semi-arid areas, Annales Geophysicae, 17, 149, https://doi.org/10.1007/s005850050744, 1999.

Feng, Y., Wang, H., Rasch, P. J., Zhang, K., Lin, W., Tang, Q., Xie, S., Hamilton, D. S., Mahowald, N., and Yu, H.: Global Dust Cycle and Direct Radiative Effect in E3SM Version 1: Impact of Increasing Model Resolution, Journal of Advances in Modeling Earth Systems, https://doi.org/10.1029/2021MS002909, 2022.

Gelaro, R., McCarty, W., Suárez, M. J., Todling, R., Molod, A., Takacs, L., Randles, C. A., Darmenov, A., Bosilovich, M. G., Reichle, R., Wargan, K., Coy, L., Cullather, R., Draper, C., Akella, S., Buchard, V., Conaty, A., da Silva, A. M., Gu, W., Kim, G. K., Koster, R., Lucchesi, R., Merkova, D., Nielsen, J. E., Partyka, G., Pawson, S., Putman, W., Rienecker, M., Schubert, S. D., Sienkiewicz, M., and Zhao, B.: The modern-era retrospective analysis for research and applications, version 2 (MERRA-2), Journal of Climate, 30, 5419–5454, https://doi.org/10.1175/JCLI-D-16-0758.1, 2017.

Gettelman, A., Mills, M. J., Kinnison, D. E., Garcia, R. R., Smith, A. K., Marsh, D. R., Tilmes, S., Vitt, F., Bardeen, C. G., McInerny, J., Liu, H. L., Solomon, S. C., Polvani, L. M., Emmons, L. K., Lamarque, J. F., Richter, J. H., Glanville, A. S., Bacmeister, J. T., Phillips, A. S., Neale, R. B., Simpson, I. R., DuVivier, A. K., Hodzic, A., and Randel, W. J.: The Whole Atmosphere Community Climate Model Version 6 (WACCM6), Journal of Geophysical Research: Atmospheres, 124, 12 380–12 403, https://doi.org/10.1029/2019JD030943, 2019.

Ginoux, P., Chin, M., Tegen, I., Prospero, J. M., Holben, B., Dubovik, O., and Lin, S. J.: Sources and distributions of dust aerosols simulated with the GOCART model, Journal of Geophysical Research Atmospheres, 106, 20 255–20 273, https://doi.org/10.1029/2000JD000053, 2001.

Ginoux, P., Prospero, J. M., Gill, T. E., Hsu, N. C., and Zhao, M.: Global-scale attribution of anthropogenic and natural dust sources and their emission rates based on MODIS Deep Blue aerosol products, Reviews of Geophysics, 50, https://doi.org/10.1029/2012RG000388, 2012.

Gliß, J., Mortier, A., Schulz, M., Andrews, E., Balkanski, Y., Bauer, S. E., Benedictow, A. M., Bian, H., Checa-Garcia, R., Chin, M., Ginoux, P., Griesfeller, J. J., Heckel, A., Kipling, Z., Kirkeväg, A., Kokkola, H., Laj, P., Le Sager, P., Tronstad Lund, M., Lund Myhre, C., Matsui, H., Myhre, G., Neubauer, D., Van Noije, T., North, P., Olivié, D. J., Rémy, S., Sogacheva, L., Takemura, T., Tsigaridis, K., and Tsyro, S. G.: AeroCom phase III multi-model evaluation of the aerosol life cycle and optical properties using ground- And space-based remote sensing as well as surface in situ observations, Atmospheric Chemistry and Physics, 21, 87–128, https://doi.org/10.5194/acp-21-87-2021, 2021.

Grini, A., Myhre, G., Zender, C. S., and Isaksen, I. S.: Model simulations of dust sources and transport in the global atmosphere: Effects of soil erodibility and wind speed variability, Journal of Geophysical Research D: Atmospheres, 110, 1–14, https://doi.org/10.1029/2004JD005037, 2005.

Hajima, T., Watanabe, M., Yamamoto, A., Tatebe, H., Noguchi, M. A., Abe, M., Ohgaito, R., Ito, A., Yamazaki, D., Okajima, H., Ito, A., Takata, K., Ogochi, K., Watanabe, S., and Kawamiya, M.: Development of the MIROC-ES2L Earth system model and the evaluation of biogeochemical processes and feedbacks, Geoscientific Model Development, 13, 2197–2244, https://doi.org/10.5194/gmd-13-2197-2020, 2020.

Huneeus, N., Schulz, M., Balkanski, Y., Griesfeller, J., Prospero, J., Kinne, S., Bauer, S., Boucher, O., Chin, M., Dentener, F., Diehl, T., Easter, R., Fillmore, D., Ghan, S., Ginoux, P., Grini, A., Horowitz, L., Koch, D., Krol, M. C., Landing, W., Liu, X., Mahowald, N., Miller, R., Morcrette, J. J., Myhre, G., Penner, J., Perlwitz, J., Stier, P., Takemura, T., and Zender, C. S.: Global dust model intercomparison in AeroCom phase i, Atmospheric Chemistry and Physics, 11, 7781–7816, https://doi.org/10.5194/acp-11-7781-2011, 2011.

Kim, D., Chin, M., Yu, H., Diehl, T., Tan, Q., Kahn, R. A., Tsigaridis, K., Bauer, S. E., Takemura, T., Pozzoli, L., Bellouin, N., Schulz, M., Peyridieu, S., Chédin, A., and Koffi, B.: Sources, sinks, and transatlantic transport of North African dust aerosol: A multimodel analysis and comparison with remote sensing data, Journal of Geophysical Research, 119, 6259–6277, https://doi.org/10.1002/2013JD021099, 2014.

Kim, D., Chin, M., Schuster, G., Yu, H., Takemura, T., Tuccella, P., Ginoux, P., Liu, X., Shi, Y., Matsui, H., Tsigaridis, K., Bauer, S. E., Kok, J. F., and Schulz, M.: Where Dust Comes From: Global Assessment of Dust Source Attributions With AeroCom Models, Journal of Geophysical Research: Atmospheres, 129, e2024JD041 377, https://doi.org/https://doi.org/10.1029/2024JD041377, 2024.

Kim, H. and Choi, M.: Impact of soil moisture on dust outbreaks in East Asia: Using satellite and assimilation data, Geophysical Research Letters, 42, 2789–2796, https://doi.org/https://doi.org/10.1002/2015GL063325, 2015.

Knippertz, P. and Todd, M. C.: Mineral dust aerosols over the Sahara: Meteorological controls on emission and transport and implications for modeling, Reviews of Geophysics, 50, https://doi.org/10.1029/2011RG000362, 2012.

Kok, J. F., Albani, S., Mahowald, N. M., and Ward, D. S.: An improved dust emission model - Part 2: Evaluation in the Community Earth System Model, with implications for the use of dust source functions, Atmospheric Chemistry and Physics, 14, 13 043–13 061, https://doi.org/10.5194/acp-14-13043-2014, 2014a.

Kok, J. F., Mahowald, N. M., Fratini, G., Gillies, J. A., Ishizuka, M., Leys, J. F., Mikami, M., Park, M. S., Park, S. U., Van Pelt, R. S., and Zobeck, T. M.: An improved dust emission model - Part 1: Model description and comparison against measurements, Atmospheric Chemistry and Physics, 14, 13 023–13 041, https://doi.org/10.5194/acp-14-13023-2014, 2014b.

Kok, J. F., Storelvmo, T., Karydis, V. A., Adebiyi, A. A., Mahowald, N. M., Evan, A. T., He, C., and Leung, D. M.: Mineral dust aerosol impacts on global climate and climate change, Nature Reviews Earth and Environment, 4, 71–86, https://doi.org/10.1038/s43017-022-00379-5, 2023.

Koster, R. D., Guo, Z., Yang, R., Dirmeyer, P. A., Mitchell, K., and Puma, M. J.: On the nature of soil moisture in land surface models, Journal of Climate, 22, 4322–4335, https://doi.org/10.1175/2009JCLI2832.1, 2009.

Leung, D. M., Kok, J. F., Li, L., Lawrence, D. M., Mahowald, N. M., Tilmes, S., and Kluzek, E.: A global dust emission dataset for estimating dust radiative forcings in climate models, Atmos. Chem. Phys., 25, 2311–2331, https://doi.org/10.5194/acp-25-2311-2025, 2025.

Li, L., Mahowald, N. M., Kok, J. F., Liu, X., Wu, M., Leung, D. M., Hamilton, D. S., Emmons, L. K., Huang, Y., Sexton, N., Meng, J., and Wan, J.: Importance of different parameterization changes for the updated dust cycle modeling in the Community Atmosphere Model (version 6.1), Geoscientific Model Development, 15, 8181–8219, https://doi.org/10.5194/gmd-15-8181-2022, 2022.

Li, L., Mahowald, N. M., Gonçalves Ageitos, M., Obiso, V., Miller, R. L., Pérez García-Pando, C., Di Biagio, C., Formenti, P., Brodrick, P. G., Clark, R. N., Green, R. O., Kokaly, R., Swayze, G., and Thompson, D. R.: Improved constraints on hematite refractive index for estimating climatic effects of dust aerosols, Communications Earth & Environment, 5, 295, https://doi.org/10.1038/s43247-024-01441-4, 2024.

Lurton, T., Balkanski, Y., Bastrikov, V., Bekki, S., Bopp, L., Braconnot, P., Brockmann, P., Cadule, P., Contoux, C., Cozic, A., Cugnet, D., Dufresne, J.-L., Éthé, C., Foujols, M.-A., Ghattas, J., Hauglustaine, D., Hu, R.-M., Kageyama, M., Khodri, M., Lebas, N., Levavasseur, G., Marchand, M., Ottlé, C., Peylin, P., Sima, A., Szopa, S., Thiéblemont, R., Vuichard, N., and Boucher, O.: Implementation

of the CMIP6 Forcing Data in the IPSL-CM6A-LR Model, Journal of Advances in Modeling Earth Systems, 12, e2019MS001 940, https://doi.org/https://doi.org/10.1029/2019MS001940, 2020.

Marticorena, B. and Bergametti, G.: Modeling the atmospheric dust cycle: 1. Design of a soil-derived dust emission scheme, Journal of Geophysical Research, 100, https://doi.org/10.1029/95jd00690, 1995.

Mauritsen, T., Bader, J., Becker, T., Behrens, J., Bittner, M., Brokopf, R., Brovkin, V., Claussen, M., Crueger, T., Esch, M., Fast, I., Fiedler, S., Fläschner, D., Gayler, V., Giorgetta, M., Goll, D. S., Haak, H., Hagemann, S., Hedemann, C., Hohenegger, C., Ilyina, T., Jahns, T., Jimenéz-de-la Cuesta, D., Jungclaus, J., Kleinen, T., Kloster, S., Kracher, D., Kinne, S., Kleberg, D., Lasslop, G., Kornblueh, L., Marotzke, J., Matei, D., Meraner, K., Mikolajewicz, U., Modali, K., Möbis, B., Müller, W. A., Nabel, J. E. M. S., Nam, C. C. W., Notz, D., Nyawira, S.-S., Paulsen, H., Peters, K., Pincus, R., Pohlmann, H., Pongratz, J., Popp, M., Raddatz, T. J., Rast, S., Redler, R., Reick, C. H., Rohrschneider, T., Schemann, V., Schmidt, H., Schnur, R., Schulzweida, U., Six, K. D., Stein, L., Stemmler, I., Stevens, B., von Storch, J.-S., Tian, F., Voigt, A., Vrese, P., Wieners, K.-H., Wilkenskjeld, S., Winkler, A., and Roeckner, E.: Developments in the MPI-M Earth System Model version 1.2 (MPI-ESM1.2) and Its Response to Increasing CO2, Journal of Advances in Modeling Earth Systems, 11, 998–1038, https://doi.org/https://doi.org/10.1029/2018MS001400, 2019.

Miller, R. L., Cakmur, R. V., Perlwitz, J., Geogdzhayev, I. V., Ginoux, P., Koch, D., Kohfeld, K. E., Prigent, C., Ruedy, R., Schmidt, G. A., and Tegen, I.: Mineral dust aerosols in the NASA Goddard Institute for Space Sciences ModelE atmospheric general circulation model, Journal of Geophysical Research Atmospheres, 111, https://doi.org/10.1029/2005JD005796, 2006.

Miller, R. L., Schmidt, G. A., Nazarenko, L. S., Bauer, S. E., Kelley, M., Ruedy, R., Russell, G. L., Ackerman, A. S., Aleinov, I., Bauer, M., Bleck, R., Canuto, V., Cesana, G., Cheng, Y., Clune, T. L., Cook, B. I., Cruz, C. A., Del Genio, A. D., Elsaesser, G. S., Faluvegi, G., Kiang, N. Y., Kim, D., Lacis, A. A., Leboissetier, A., LeGrande, A. N., Lo, K. K., Marshall, J., Matthews, E. E., McDermid, S., Mezuman, K., Murray, L. T., Oinas, V., Orbe, C., Pérez García-Pando, C., Perlwitz, J. P., Puma, M. J., Rind, D., Romanou, A., Shindell, D. T., Sun, S., Tausnev, N., Tsigaridis, K., Tselioudis, G., Weng, E., Wu, J., and Yao, M. S.: CMIP6 Historical Simulations (1850–2014) With GISS-E2.1, Journal of Advances in Modeling Earth Systems, 13, https://doi.org/10.1029/2019MS002034, 2021.

Nandintsetseg, B. and Shinoda, M.: Land surface memory effects on dust emission in a Mongolian temperate grassland, Journal of Geophysical Research: Biogeosciences, 120, 414–427, https://doi.org/10.1002/2014JG002708, 2015.

Peng, Y., Von Salzen, K., and Li, J.: Simulation of mineral dust aerosol with Piecewise Log-normal Approximation (PLA) in CanAM4-PAM, Atmospheric Chemistry and Physics, 12, 6891–6914, https://doi.org/10.5194/acp-12-6891-2012, 2012.

Prospero, J. M. and Lamb, P. J.: African Droughts and Dust Transport to the Caribbean: Climate Change Implications, Science, 302, 1024–1027, https://doi.org/10.1126/science.1089915, 2003.

Prospero, J. M., Ginoux, P., Torres, O., Nicholson, S. E., and Gill, T. E.: Environmental characterization of global sources of atmospheric soil dust identified with the Nimbus 7 Total Ozone Mapping Spectrometer (TOMS) absorbing aerosol product, Reviews of Geophysics, 40, 2–1, https://doi.org/10.1029/2000RG000095, 2002.

Pu, B. and Ginoux, P.: The impact of the Pacific Decadal Oscillation on springtime dust activity in Syria, Atmospheric Chemistry and Physics, 16, 13 431–13 448, https://doi.org/10.5194/acp-16-13431-2016, 2016.

Pu, B. and Ginoux, P.: How reliable are CMIP5 models in simulating dust optical depth?, Atmospheric Chemistry and Physics, 18, 12 491–12 510, https://doi.org/10.5194/acp-18-12491-2018, 2018.

Randles, C. A., da Silva, A. M., Buchard, V., Colarco, P. R., Darmenov, A., Govindaraju, R., Smirnov, A., Holben, B., Ferrare, R., Hair, J., Shinozuka, Y., and Flynn, C. J.: The MERRA-2 aerosol reanalysis, 1980 onward. Part I: System description and data assimilation evaluation, Journal of Climate, 30, 6823–6850, https://doi.org/10.1175/JCLI-D-16-0609.1, 2017.

RAVI, S., ZOBECK, T. E. D. M., OVER, T. M., OKIN, G. S., and D'ODORICO, P.: On the effect of moisture bonding forces in air-dry soils on threshold friction velocity of wind erosion, Sedimentology, 53, 597–609, https://doi.org/https://doi.org/10.1111/j.1365-3091.2006.00775.x, 2006.

Ridley, D. A., Heald, C. L., Pierce, J. R., and Evans, M. J.: Toward resolution-independent dust emissions in global models: Impacts on the seasonal and spatial distribution of dust, Geophysical Research Letters, 40, 2873–2877, https://doi.org/10.1002/grl.50409, 2013.

Rind, D., Orbe, C., Jonas, J., Nazarenko, L., Zhou, T., Kelley, M., Lacis, A., Shindell, D., Faluvegi, G., Romanou, A., Russell, G., Tausnev, N., Bauer, M., and Schmidt, G.: GISS Model E2.2: A Climate Model Optimized for the Middle Atmosphere—Model Structure, Climatology, Variability, and Climate Sensitivity, Journal of Geophysical Research: Atmospheres, 125, https://doi.org/10.1029/2019JD032204, 2020.

Roberts, M. J., Baker, A., Blockley, E. W., Calvert, D., Coward, A., Hewitt, H. T., Jackson, L. C., Kuhlbrodt, T., Mathiot, P., Roberts, C. D., Schiemann, R., Seddon, J., Vannière, B., and Vidale, P. L.: Description of the resolution hierarchy of the global coupled HadGEM3-GC3.1 model as used in CMIP6 HighResMIP experiments, Geosci. Model Dev., 12, 4999–5028, https://doi.org/10.5194/gmd-12-4999-2019, 2019.

Séférian, R., Nabat, P., Michou, M., Saint-Martin, D., Voldoire, A., Colin, J., Decharme, B., Delire, C., Berthet, S., Chevallier, M., Sénési, S., Franchisteguy, L., Vial, J., Mallet, M., Joetzjer, E., Geoffroy, O., Guérémy, J. F., Moine, M. P., Msadek, R., Ribes, A., Rocher, M., Roehrig, R., Salas-y Mélia, D., Sanchez, E., Terray, L., Valcke, S., Waldman, R., Aumont, O., Bopp, L., Deshayes, J., Éthé, C., and Madec, G.: Evaluation of CNRM Earth System Model, CNRM-ESM2-1: Role of Earth System Processes in Present-Day and Future Climate, Journal of Advances in Modeling Earth Systems, 11, 4182–4227, https://doi.org/10.1029/2019MS001791, 2019.

Seland, O., Bentsen, M., Olivié, D., Toniazzo, T., Gjermundsen, A., Graff, L. S., Debernard, J. B., Gupta, A. K., He, Y. C., Kirkeväg, A., Schwinger, J., Tjiputra, J., Schanke Aas, K., Bethke, I., Fan, Y., Griesfeller, J., Grini, A., Guo, C., Ilicak, M., Karset, I. H. H., Landgren, O., Liakka, J., Moseid, K. O., Nummelin, A., Spensberger, C., Tang, H., Zhang, Z., Heinze, C., Iversen, T., and Schulz, M.: Overview of the Norwegian Earth System Model (NorESM2) and key climate response of CMIP6 DECK, historical, and scenario simulations, Geoscientific Model Development, 13, 6165–6200, https://doi.org/10.5194/gmd-13-6165-2020, 2020.

Shao, Y., Raupach, M. R., and Leys, J. F.: A model for predicting aeolian sand drift and dust entrainment on scales from paddock to region, Australian Journal of Soil Research, 34, 309–342, https://doi.org/10.1071/SR9960309, 1996.

Shao, Y., Wyrwoll, K. H., Chappell, A., Huang, J., Lin, Z., McTainsh, G. H., Mikami, M., Tanaka, T. Y., Wang, X., and Yoon, S.: Dust cycle: An emerging core theme in Earth system science, Aeolian Research, 2, 181–204, https://doi.org/10.1016/j.aeolia.2011.02.001, 2011.

Shevliakova, E., Malyshev, S., Martinez-Cano, I., Milly, P. C. D., Pacala, S. W., Ginoux, P., Dunne, K. A., Dunne, J. P., Dupuis, C., Findell, K. L., Ghannam, K., Horowitz, L. W., Knutson, T. R., Krasting, J. P., Naik, V., Phillipps, P., Zadeh, N., Yu, Y., Zeng, F., and Zeng, Y.: The Land Component LM4.1 of the GFDL Earth System Model ESM4.1: Model Description and Characteristics of Land Surface Climate and Carbon Cycling in the Historical Simulation, Journal of Advances in Modeling Earth Systems, 16, e2023MS003 922, https://doi.org/https://doi.org/10.1029/2023MS003922, 2024.

Shinoda, M., Gillies, J. A., Mikami, M., and Shao, Y.: Temperate grasslands as a dust source: Knowledge, uncertainties, and challenges, Aeolian Research, 3, 271–293, https://doi.org/10.1016/j.aeolia.2011.07.001, 2011.

Sigmond, M., Anstey, J., Arora, V., Digby, R., Gillett, N., Kharin, V., Merryfield, W., Reader, C., Scinocca, J., Swart, N., Virgin, J., Abraham, C., Cole, J., Lambert, N., Lee, W. S., Liang, Y., Malinina, E., Rieger, L., Von Salzen, K., Seiler, C., Seinen, C., Shao, A., Sospedra-Alfonso, R., Wang, L., and Yang, D.: Improvements in the Canadian Earth System Model (CanESM) through systematic model analysis: CanESM5.0 and CanESM5.1, Geoscientific Model Development, 16, 6553–6591, https://doi.org/10.5194/gmd-16-6553-2023, 2023.

Sokolik, I. N., Darmenova, K., Huang, J., Kalashnikova, O., Kurosaki, Y., and Xi, X.: Examining changes in land cover and land use, regional climate and dust in Dryland East Asia and Their Linkages within the Earth System, in: Dryland East Asia: Land Dynamics amid Social and Climate Change, edited by Chen, J., Wan, S., Henebry, G., Qi, J., Gutman, G., Sun, G., and Kappas, M., chap. 9, pp. 183–211, DE GRUYTER, Berlin, Boston, ISBN 9783110287912, https://doi.org/10.1515/9783110287912.183, 2021.

Takemura, T., Egashira, M., Matsuzawa, K., Ichijo, H., O'Ishi, R., and Abe-Ouchi, A.: A simulation of the global distribution and radiative forcing of soil dust aerosols at the Last Glacial Maximum, Atmospheric Chemistry and Physics, 9, 3061–3073, https://doi.org/10.5194/acp-9-3061-2009, 2009.

Tatebe, H., Ogura, T., Nitta, T., Komuro, Y., Ogochi, K., Takemura, T., Sudo, K., Sekiguchi, M., Abe, M., Saito, F., Chikira, M., Watanabe, S., Mori, M., Hirota, N., Kawatani, Y., Mochizuki, T., Yoshimura, K., Takata, K., O'Ishi, R., Yamazaki, D., Suzuki, T., Kurogi, M., Kataoka, T., Watanabe, M., and Kimoto, M.: Description and basic evaluation of simulated mean state, internal variability, and climate sensitivity in MIROC6, Geoscientific Model Development, 12, 2727–2765, https://doi.org/10.5194/gmd-12-2727-2019, 2019.

Tegen, I., Harrison, S. P., Kohfeld, K., Prentice, I. C., Coe, M., and Heimann, M.: Impact of vegetation and preferential source areas on global dust aerosol: Results from a model study, Journal of Geophysical Research Atmospheres, 107, https://doi.org/10.1029/2001JD000963, 2002.

Tegen, I., Neubauer, D., Ferrachat, S., Drian, C. S. L., Bey, I., Schutgens, N., Stier, P., Watson-Parris, D., Stanelle, T., Schmidt, H., Rast, S., Kokkola, H., Schultz, M., Schroeder, S., Daskalakis, N., Barthel, S., Heinold, B., and Lohmann, U.: The global aerosol-climate model echam6.3-ham2.3 -Part 1: Aerosol evaluation, Geoscientific Model Development, 12, 1643–1677, https://doi.org/10.5194/gmd-12-1643-2019, 2019.

Textor, C., Schulz, M., Guibert, S., Kinne, S., Balkanski, Y., Bauer, S., Berntsen, T., Berglen, T., Boucher, O., Chin, M., Dentener, F., Diehl, T., Easter, R., Feichter, H., Fillmore, D., Ghan, S., Ginoux, P., Gong, S., Grini, A., Hendricks, J., Horowitz, L., Huang, P., Isaksen, I., Iversen, T., Kloster, S., Koch, D., Kirkevåg, A., Kristjansson, J. E., Krol, M., Lauer, A., Lamarque, J. F., Liu, X., Montanaro, V., Myhre, G., Penner, J., Pitari, G., Reddy, S., Seland, Stier, P., Takemura, T., and Tie, X.: Analysis and quantification of the diversities of aerosol life cycles within AeroCom, Atmospheric Chemistry and Physics, 6, 1777–1813, https://doi.org/10.5194/acp-6-1777-2006, 2006.

Van Noije, T., Bergman, T., Le Sager, P., O'Donnell, D., Makkonen, R., Gonçalves-Ageitos, M., Döscher, R., Fladrich, U., Von Hardenberg, J., Keskinen, J. P., Korhonen, H., Laakso, A., Myriokefalitakis, S., Ollinaho, P., Pérez Garciá-Pando, C., Reerink, T., Schrödner, R., Wyser, K., and Yang, S.: EC-Earth3-AerChem: A global climate model with interactive aerosols and atmospheric chemistry participating in CMIP6, Geoscientific Model Development, 14, 5637–5668, https://doi.org/10.5194/gmd-14-5637-2021, 2021.

Volodin, E. M.: Possible Climate Change in Russia in the 21st Century Based on the INM-CM5-0 Climate Model, Russian Meteorology and Hydrology, 47, 327–333, https://doi.org/10.3103/S1068373922050016, 2022.

Volodin, E. M. and Kostrykin, S. V.: The aerosol module in the INM RAS climate model, Russian Meteorology and Hydrology, 41, 519–528, https://doi.org/10.3103/S106837391608001X, 2016.

Woodward, S.: Modeling the atmospheric life cycle and radiative impact of mineral dust in the Hadley Centre climate model, Journal of Geophysical Research Atmospheres, 106, 18 155–18 166, https://doi.org/10.1029/2000JD900795, 2001.

Woodward, S.: Hadley Centre Technical Note 87 - Mineral dust in HadGEM2, Tech. rep., Met Office, Exeter, 2011.

Woodward, S., Sellar, A. A., Tang, Y., Stringer, M., Yool, A., Robertson, E., and Wiltshire, A.: The simulation of mineral dust in the United Kingdom Earth System Model UKESM1, Atmospheric Chemistry and Physics, 22, 14 503–14 528, https://doi.org/10.5194/acp-22-14503-2022, 2022.

Wu, C., Lin, Z., Liu, X., Li, Y., Lu, Z., and Wu, M.: Can Climate Models Reproduce the Decadal Change of Dust Aerosol in East Asia?, Geophysical Research Letters, 45, 9953–9962, https://doi.org/10.1029/2018GL079376, 2018.

Wu, C., Lin, Z., and Liu, X.: The global dust cycle and uncertainty in CMIP5 (Coupled Model Intercomparison Project phase 5) models, Atmospheric Chemistry and Physics, 20, 10 401–10 425, https://doi.org/10.5194/acp-20-10401-2020, 2020.

Xi, X.: On the Geomorphic, Meteorological, and Hydroclimatic Drivers of the Unusual 2018 Early Summer Salt Dust Storms in Central Asia, Journal of Geophysical Research: Atmospheres, 128, https://doi.org/10.1029/2022JD038089, 2023.

Xi, X. and Sokolik, I. N.: Seasonal dynamics of threshold friction velocity and dust emission in Central Asia, Journal of Geophysical Research: Atmospheres, 120, 1536–1564, https://doi.org/10.1002/2014JD022471, 2015a.

Xi, X. and Sokolik, I. N.: Dust interannual variability and trend in Central Asia from 2000 to 2014 and their climatic linkages, Journal of Geophysical Research: Atmospheres, 120, 12 175–12 197, https://doi.org/10.1002/2015JD024092, 2015b.

Xie, S., Terai, C., Wang, H., Tang, Q., Fan, J., Burrows, S., Lin, W., Wu, M., Song, X., Zhang, Y., Taylor, M., Golaz, J.-C., Benedict, J., Chen, C.-C., Feng, Y., Hannah, W., Ke, Z., Shan, Y., Larson, V., and Bader, D.: The Energy Exascale Earth System Model Version 3. Part I: Overview of the Atmospheric Component, Under Review, https://doi.org/10.22541/essoar.174456922.21825772/v1, 2025.

Yukimoto, S., Kawai, H., Koshiro, T., Oshima, N., Yoshida, K., Urakawa, S., Tsujino, H., Deushi, M., Tanaka, T., Hosaka, M., Yabu, S., Yoshimura, H., Shindo, E., Mizuta, R., Obata, A., Adachi, Y., and Ishii, M.: The meteorological research institute Earth system model version 2.0, MRI-ESM2.0: Description and basic evaluation of the physical component, Journal of the Meteorological Society of Japan, 97, 931–965, https://doi.org/10.2151/jmsj.2019-051, 2019.

Yumimoto, K., Tanaka, T. Y., Oshima, N., and Maki, T.: JRAero: The Japanese Reanalysis for Aerosol v1.0, Geoscientific Model Development, 10, 3225–3253, https://doi.org/10.5194/gmd-10-3225-2017, 2017.

Zender, C. S. and Kwon, E. Y.: Regional contrasts in dust emission responses to climate, Journal of Geophysical Research Atmospheres, 110, https://doi.org/10.1029/2004JD005501, 2005.

Zender, C. S., Bian, H., and Newman, D.: Mineral Dust Entrainment and Deposition (DEAD) model: Description and 1990s dust climatology, Journal of Geophysical Research: Atmospheres, 108, https://doi.org/10.1029/2002jd002775, 2003.

Zhang, J., Teng, Z., Huang, N., Guo, L., and Shao, Y.: Surface renewal as a significant mechanism for dust emission, Atmospheric Chemistry and Physics, 16, 15 517–15 528, https://doi.org/10.5194/acp-16-15517-2016, 2016a.

Zhang, K., Zhao, C., Wan, H., Qian, Y., Easter, R. C., Ghan, S. J., Sakaguchi, K., and Liu, X.: Quantifying the impact of sub-grid surface wind variability on sea salt and dust emissions in CAM5, Geoscientific Model Development, 9, 607–632, https://doi.org/10.5194/gmd-9-607-2016, 2016b.

Zhao, A., Ryder, C. L., and Wilcox, L. J.: How well do the CMIP6 models simulate dust aerosols?, Atmospheric Chemistry and Physics, 22, 2095–2119, https://doi.org/10.5194/acp-22-2095-2022, 2022.

Zomer, R. J., Xu, J., and Trabucco, A.: Version 3 of the Global Aridity Index and Potential Evapotranspiration Database, Scientific Data, 9, https://doi.org/10.1038/s41597-022-01493-1, 2022.

Zou, X. K. and Zhai, P. M.: Relationship between vegetation coverage and spring dust storms over northern China, Journal of Geophysical Research: Atmospheres, 109, https://doi.org/10.1029/2003jd003913, 2004.